Scanning Microscopy

Volume 8 | Number 2 Article 1

7-22-1994

Detection of Topographic Contrast in the Scanning Electron Microscope at Low and Medium Resolution by Different Detectors and Detector Systems

J. Hejna
Technical University of Wrocław

Scanning Microscopy, Vol. 8, No. 2, 1994 (Pages 143-164) 0891-7035/94$5.00+.25
Scanning Microscopy International, Chicago (AMF O'Hare), IL 60666 USA

DETECTION OF TOPOGRAPHIC CONTRAST IN THE SCANNING ELECTRON MICROSCOPE AT LOW AND MEDIUM RESOLUTION BY DIFFERENT DETECTORS AND DETECTOR SYSTEMS

J. Hejna

Institute of Electron Technology, Technical University of Wrocław,
Wybrzeże Wyspiańskiego 27, 50-370 Wrocław, Poland

Telephone Number: 48-71-202879; FAX Number: 48-71-213504

(Received for publication January 3, 1994 and in revised form July 22, 1994)

Abstract

Origins of topographic contrast in the scanning electron microscope (SEM) are different at different resolution levels. At low resolution, tilt contrast of large features dominates; at medium resolution, diffusion contrast of features smaller than an interaction volume of primary electrons dominates.

The secondary electron (SE) signal, commonly used in the SEM, does not give a good tilt contrast; better contrast can be obtained with backscattered electron (BSE) signal of a converter and a sector-shaped ring detector. For obtaining topographic images from signals containing topographic and material contrast, signals of detector systems containing two or more detectors are mixed. Detector systems containing BSE detectors give more reproducible signals with a more uniform dependence on tilt angles than systems containing SE detectors. Tilt contrast of specimens coated with thin layers of heavy metals is similar to the contrast of uncoated specimens in the case of an SE detector, and better tilt contrast can be obtained with a sector-shaped ring BSE detector.

Diffusion contrast dominates at medium resolution. Contrast obtained with three selected detectors: SE detector, sector-shaped ring BSE detector, annular top BSE detector, is also discussed. The contrast is lowest for the top BSE detector and highest in the case of SE detection, especially for materials of low density. In the case of coated specimens, the SE detector and the sector-shaped ring BSE detector give good contrast and both are suitable for medium resolution studies.

The discussion in the paper concerns untilted or slightly tilted specimens.

Key Words: Scanning electron microscopy, low resolution, medium resolution, electron detectors, detector systems, topographic contrast.

Introduction

The low and medium resolution modes of scanning electron microscope (SEM) operation concern work outside the range of high resolution imaging. The high resolution mode, as understood here, is restricted to a case of work close to the physical limit of resolution of the SEM. The ultimate resolution of the SEM depends on the escape depth of electrons being detected and on the delocalization of their generation process and can be obtained when the diameter of the primary beam is small enough. The high resolution imaging in the SEM is not fully understood yet, and a limit for the beam diameter can be set to 0.5-2 nm, depending on the specimen material. Conditions for high resolution imaging and contrast mechanisms of this mode of SEM operation were discussed in papers of Matsukawa and Shimizu (1974), Liu and Cowley (1988), Ding and Shimizu (1989), Joy (1991), Joy and Pawley (1992), Wells and Nacucchi (1992) and many others. For the purpose of this paper, we can say that low and medium resolution modes of SEM operation concern imaging of features larger than about 10-20 nm with a beam diameter larger than about 2 nm.

For obtaining topographic and material contrast in the SEM, secondary electrons (SE) and backscattered electrons (BSE) are used. SE are generated by the primary beam at the point of impact and by BSE escaping from the specimen (Kanter, 1961; Schur *et al.*, 1967; Drescher *et al.*, 1970). They are called SE1 and SE2, respectively. Among BSE, there are some which are scattered in one high angle event at the impact point of the primary beam (Wells, 1977), which can be called, by analogy, BSE1. However, the number of BSE1 is very small and they can form images only if some special means for their detection are undertaken; usually, all BSE are detected, and the influence of BSE1 is negligible. The emission areas of SE1 and BSE1 on a flat specimen surface are comparable with the diameter of the primary beam (Joy, 1984; Kotera, 1989); those of the majority of BSE and of SE2 are comparable with the range of primary electrons in the specimen (Heidenreich

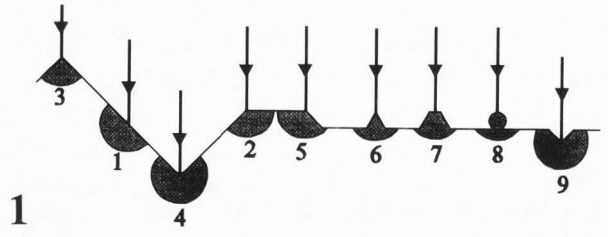

1

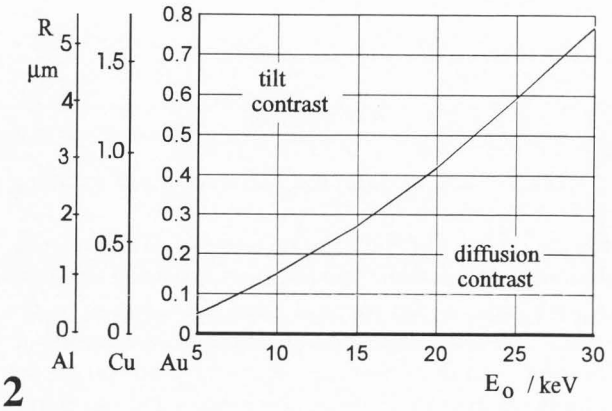

2

Figure 1. Some features giving topographic contrast in the SEM. **1**: feature larger than the interaction volume; **2**: edge, **3**: ridge and **4**: valley, bordering the surfaces; **5** to **9**: features smaller than the interaction volume: **5**: step, **6** and **7**: bars, **8**: particle, and **9**: groove. The primary beam and its interaction volume in the material is shown for each feature.

Figure 2. The dependence of electron range on the primary beam energy for three elements and approximate regions of dominating tilt or diffusion contrast.

---

and Thompson, 1973; Murata *et al.*, 1980; Hasselbach, 1988). In the typical range of accelerating voltages of the SEM, from about 5 kV to 30-40 kV, the electron range is much larger than the primary beam diameter. Also, the information depth (the thickness of a layer from which information is present in the signal) differs significantly for different categories of electrons. For SE1, it is lower than 10 nm; for the majority of BSE and SE2, it is equal to about half the electron range. Though SE2 escape from the depth of about 10 nm, they are BSE dependent, and their information depth is the same as BSE. The high resolution contrast is caused by SE1 and BSE1 and can be achieved only in the case when the beam diameter is small enough. At low primary beam energies, the situation is different: emission areas and information depths of SE1, SE2 and BSE merge, and all SE and BSE contribute to low, medium and high resolution images.

In the present paper, detection of topographic contrast at low and medium resolution for primary beam energies larger than 5 keV is discussed. The material contrast accompanies usually the topographic contrast, and its detection is also mentioned. After a short discussion of origins of topographic and material contrast, the detectors and detector systems for SE and BSE detection in the SEM are described. Methods of testing the detectors and detector systems are discussed, and some results of tests are presented. To demonstrate how an appearance of an image depends on the detector used for imaging, micrographs of different specimens recorded with selected detectors are shown. The discussion concerns untilted or slightly tilted specimens.

Origins of Topographic and Material Contrasts in the SEM

Figure 1 shows some of the topographic features which produce topographic contrast in the SEM. Depending on their dimensions, different phenomena contribute to the signal.

When surface features composed of uniform material are larger than an interaction volume of the primary beam in the specimen (dimensions larger than an electron range, feature 1 in Fig. 1), the following phenomena contribute to the signal:

- The increase of the SE yield, δ, and the BSE coefficient, η, with increasing surface inclination angle (Reimer and Seidel, 1968; Arnal *et al.*, 1969), resulting in topographic tilt contrast.

- The increase of η with increasing atomic number of the specimen material (Palluel, 1947; Bishop, 1966; Heinrich, 1966; Wittry, 1966), resulting in material or Z contrast.

- The change of the angular distribution of BSE from a cosine law at normal incidence of the primary beam to an elongated distribution with reflection-like maximum at tilted incidence (Kanter, 1957; Reimer and Pfefferkorn, 1973; Darlinski, 1981). This influences the tilt contrast in BSE images.

- The enhanced emission of SE and BSE at edges and ridges bordering the surfaces (features 2 and 3 in Fig. 1), resulting in edge contrast.

When surface features and surface and volume inhomogeneities are smaller than the interaction volume (dimensions smaller than the electron range), the following phenomena take place:

- When features protrude from the surface (features from 5 to 8 in Fig. 1), they are wholly immersed in the diffusion cloud, and more BSE can escape and also produce more SE2 (diffusion contrast).

- When grooves and holes are present on the surface (feature 9 in Fig. 1), the SE and BSE emission decrease because the diffusion cloud is shifted deeper into the specimen.

- If the composition of the specimen is not uniform inside an interaction volume (thin layers, inclusions of

one material in a matrix of another material, small features of one material lying on the surface of another material), material contrast is modified and can range from zero to the value characteristic for a uniform specimen.

Figure 2 shows the dependence of electron range on primary beam energy for some metals. The relation of Cosslett and Thomas (1964) and Hunger and Rogaschewski (1986) in the form $R = 9*E^{1.5}$ was used (R is the electron range in $\mu g/cm^2$ and E is the electron energy in keV). As we can see from Figure 2, the topographic tilt contrast and the pure material contrast dominate for relatively large features (especially in the case of materials of low density).

Discussed above are types of emission contrast originating from the emission properties of the specimen. These contrasts are modulated by the detection characteristics of a detector (solid angle of the signal collection and its correspondence with an angular distribution of emitted electrons, sensitivity of the detector to electrons with different energies) and by the specimen itself (shielding of one feature by others, SE and BSE emission from areas remote from the point of impact, struck by backscattered or transmitted electrons). The SE signal can also contain electrons emitted from different parts of specimen chamber struck by BSE (mainly from the lens polepiece).

Detectors for Topographic and Material Contrast

An ideal detector should be sensitive to a particular contrast only and should not introduce additional noise to the signal. Usually the detector signal is a mixture of different types of contrasts, and the detector increases the noise. Knowing the performances of detectors, we can make the best use of the electron-specimen interaction by choosing appropriate detector or detector systems for specific applications (Reimer, 1984).

Although, in the first studies on the development of the SEM instrument (at Cambridge University, McMullan, 1953), BSE detection was utilized, real progress was achieved when an efficient SE detector was developed (Everhart and Thornley, 1960; E-T detector; Fig. 3). This detector not only collects electrons emitted from the specimen surface (SE1 and SE2) but also SE generated by BSE in the specimen chamber (SE3) and by primaries at the final aperture (SE4) (Everhart *et al.*, 1959; Schur *et al.*, 1967; Drescher *et al.*, 1970; Peters, 1982; Oatley, 1983). The amount of SE4 is usually small (several percent of the total SE signal), but the amount of SE3 can be relatively large. Everhart *et al.* (1959) and Drescher *et al.* (1970) estimated that SE3 form typically about 30 % of the total SE signal. Sometimes, depending on the geometry of the specimen chamber and on the specimen material, this value can be larger than 50% (Oatley, 1983) and it even can rise to 60-70% of the total SE signal (Peters, 1984). The electric field of the detector attracts slow SE, and the position of the detector is not critical. Everhart and Thornley used a hemispherical plastic scintillator coupled to a perspex light-guide. Hatzakis (1970) and Taylor (1972) covered hemispherical endings of perspex and quartz light-guides, respectively, with thin layers of scintillating plastic. The main disadvantage of the plastic scintillator in the SE detector is its low resistance to radiation damage which results in a short life time. Marshall and Stephen (1972) used lithium activated glass instead of plastic. Secker *et al.* (1973) made a thin layer scintillator from a luminescent phosphor powder. One of such powders with the symbol P-47 (yttrium-silicate doped with Ce) found widespread use in SE detectors. Pawley (1974) reported the use of a single-crystal of yttrium-aluminium garnet (YAG); further studies on this material, leading to its widespread use, were conducted by Autrata *et al.* (1978). Autrata *et al.* (1983a) introduced single crystal yttrium-aluminium perovskite (YAP) scintillators. Schauer and Autrata (1979, 1992) studied light propagation in the single-crystal scintillator-light-guide combination and Autrata (1990) optimized the design of the Everhart-Thornley detector (ETD) with the single-crystal scintillator. Besides SEM instruments, ETD was also implemented in scanning transmission EMs (Koike *et al.*, 1971). At present, thin-layer powder scintillators and single-crystal scintillators are mainly used in ETD. Usually, the current at the output of the photomultiplier is amplified and used for imaging. The noise of the photomultiplier and an analog electronic circuitry impairs the signal-to-noise ratio, especially in the case of a weak signal. To avoid this disadvantage, Yamada *et al.* (1991) used digital single pulse counting at the output of the photomultiplier, and a rate of electron counts as a signal. Noise pulses have smaller amplitudes than signal pulses and are filtered-out by a discriminator. Uchikawa *et al.* (1992) claimed an improvement of the signal-to-noise ratio from 3 to 4 times in comparison to the conventional method. Instead of the scintillator-photomultiplier combination, Hughes *et al.* (1967) proposed a channel electron multiplier and Crewe *et al.* (1970) a semiconductor diode at high potential for detection of SE in an ultra-high vacuum SEM chamber.

Detection of BSE found widespread use as more efficient detectors than that of McMullan (1953) became available. BSE offer some advantages in comparison to SE: strong material dependency of η, easy manipulation of the appearance of topographic contrast by placing the detector at an optimum position, and insensitivity of BSE trajectories to electric and magnetic fields inside a specimen chamber of the SEM. Figure 4 shows possible detector positions for untilted (or slightly-tilted) and highly-tilted specimens.

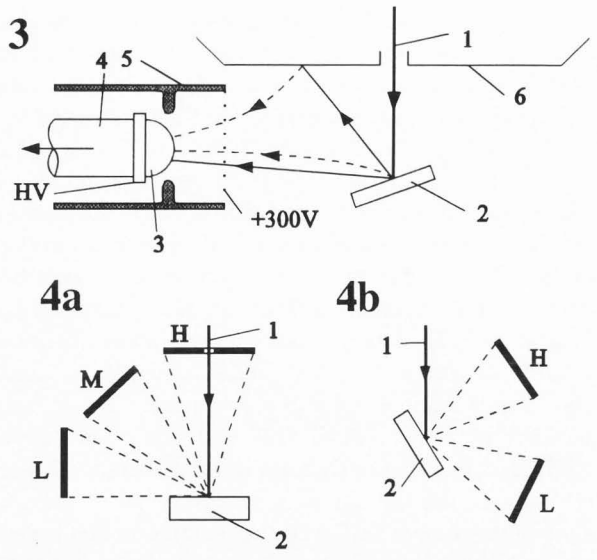

Figure 3. Everhart-Thornley detector (ETD) for SE. **1**: Primary beam, **2**: specimen, **3**: scintillator, **4**: light-guide, **5**: cage with a grid, **6**: lens pole-piece, HV: high voltage to the scintillator, dashed lines: trajectories of SE, full lines: trajectories of BSE, arrow shows direction to the photomultiplier.

Figure 4. Possible positions of BSE detectors in the SEM for untilted or slightly tilted specimens (**a**) and for highly tilted specimens (**b**). H: high position, L: low position, M: medium position, 1: primary beam, 2: specimen.

In the case of an untilted specimen, the detector (small or large solid angle) can be placed at high, medium or low position. First experiments with the high take-off detector were conducted by McMullan (1953) with an electron multiplier and by Wells with a scintillation detector (Wells: PhD Thesis, 1957; cited in Wells, 1979). The first commercial BSE detector was that of Kimoto and coworkers (Kimoto *et al.*, 1965; Kimoto and Hashimoto, 1966) who introduced a pair of small area semiconductor diodes (Fig. 5a). Further progress was achieved when Wolf and Everhart (1969) built an efficient annular solid state detector (SSD) of large solid angle (Fig. 5b). Griffiths *et al.* (1972) introduced a multichannel-plate electron multiplier as the BSE detector, it was an annular-split form (Fig. 5c), similar to the SSD of Munden *et al.* (1973). Robinson (1975) introduced the wide-angle plastic scintillator detector (Fig. 5d) and Autrata *et al.* (1983b) applied single-crystal YAG and YAP scintillators to this design. Moll *et al.* (1978) made use of the SE generated by BSE at the lens pole-piece for indirect detection of BSE signal (Fig. 5e); SE from the specimen were suppressed by a negatively biased grid, placed over the specimen. Boyde and Cowham (1980) worked in a conversion mode of BSE detection without a grid but with positive biasing of the specimen. Reimer and Volbert (1979) improved the conversion efficiency by placing a plate covered with MgO under the lens polepiece (Fig. 5f). The plate can be biased negatively or positively in respect to the grid in front of it, which allows to switch SE3 on or off. Though conversion takes place in high position, ETD collects converted SE emitted in its vicinity with higher efficiency. Converters are highly directional detectors and can be treated as detectors shifted to one side of the beam, even to a medium position (depending on the size of the converting surface).

An ETD with a negatively biased entrance grid works as a detector of a small solid angle in a low position. Such a detector has a very poor signal-to-noise ratio, and, in order to make this type of detector more efficient, Wells and Bremer (1970) used a scintillator of large solid angle (Fig. 5g). Chang (1974) used a pair of scintillators at two sides of the specimen; Walker and Booker (1976) placed a metal foil between the specimen and the scintillator as a filter absorbing BSE of lower energy. Besides plastic, powder and single crystal YAG and YAP scintillators used in such detectors, Takahashi (1977) reported the use of a layer of CdS and Fitch *et al.* (1984) a single crystal of CaF_2 as scintillator materials. In order to detect BSE at low position with the highest efficiency, Hejna (1987) built a ring detector surrounding the specimen (Fig. 5h). This design was subsequently optimized for a better tilt contrast (Hejna, 1988) (sector-shaped ring in Fig. 5i).

The medium position is an intermediate one between low and high positions, and some designs of a converter and some designs of solid-state detectors with diodes placed at larger distances from the beam can belong to this group. Also the multifunction detector (MFD) of Kuypers and Lichtenegger (1980) (Fig. 5j) which can contain up to four scintillators around the primary beam belongs to this category.

Some detectors can subtend large solid angles and cannot be treated as detectors placed at one of the earlier-mentioned positions. For example, large top detectors (solid-state diodes, scintillators, multichannel multipliers (Figs. 5b, 5c and 5d)) can extend over high and medium positions; large side detectors (e.g., large disc or sector-shaped ring scintillators (Figs. 5g and 5i)) can extend over low and medium positions.

The response of a detector to striking electrons differs for different types of detectors. The signals of semiconductor and scintillation detectors are proportional to the energy of the electron lowered by a threshold energy of the detector (usually 1-3 keV). These detectors are more sensitive to electrons with higher energies. The signal of SE3 generated in the pole-piece (conversion mode of Moll) decreases with increasing electron

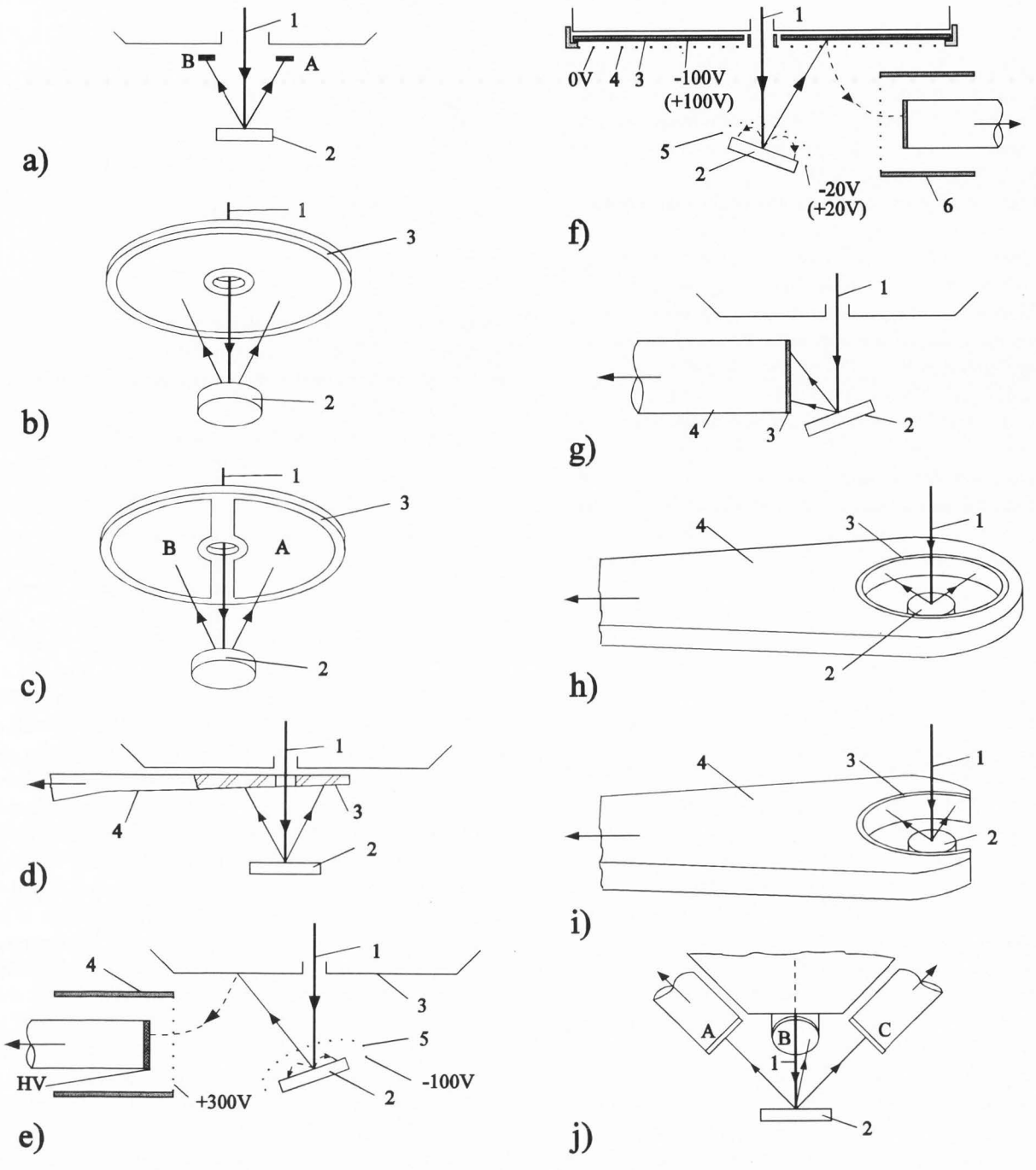

Figure 5. BSE detectors for SEM (1: primary beam and 2: specimen in each drawing). (**a**) Small area semiconductor diodes, A and B; (**b**) large area annular semiconductor detector or multichannel electron multiplier (channel plate), 3: detector; (**c**) large area annular channel plate or semiconductor detector split into two halves, A and B (can be divided also into four quadrants), 3: detector; (**d**) wide angle scintillation detector, 3: scintillator (plastic or single-crystal), 4: light-guide (perspex or the same piece of scintillation plastic), (**e**) detection of BSE by conversion to SE at the lens pole-piece, 3: pole-piece, 4: ETD, 5: grid suppressing SE, full line: trajectory of BSE, dashed line: trajectory of SE; (**f**) detection of BSE by conversion to SE at a plate covered with MgO, 3: plate, 4: grid passing or retarding converted electrons, 5: grid passing or retarding SE from the specimen, 6: ETD (voltages without parentheses concern detection of BSE, those in parentheses detection of SE with SE3 suppressed); (**g**) large area scintillation detector at one side of the specimen, 3: scintillator, 4: light-guide; (**h**) ring scintillation detector, 3: scintillator, 4: light-guide; (**i**) sector-shaped ring scintillation detector, 3: scintillator, 4: light-guide; and (**j**) multifunction detector with up to four scintillation detectors (three shown: A, B and C) at medium positions.

energy due to the decrease of the SE yield (Drescher *et al.*, 1970). The converter, using a plate covered with MgO, has a constant signal in a wide range of primary beam energies (1-20 keV). Channel plate multipliers are more sensitive to low energy electrons and are good detectors in low voltage SEM.

Noise of different detectors was studied by Baumann and Reimer (1981) and Oatley (1981). The noise of an ETD increases a little with primary beam energy; the noise of an unbiased scintillator of large solid angle is very high at low energies and drops fast with increasing energy; the noise of the converter is nearly constant at different energies.

Besides detectors at fixed positions, some investigators used movable ones which can be placed at any position. Blaschke and Schur (1974) used a movable semiconductor detector, Reimer *et al.* (1978) used a movable scintillation detector, and Kikuchi and Takashima (1978) used a pair of large area semiconductor detectors on a pivoted arm. Integrated design of two detectors at different take-off angles is described by Autrata (1984).

In the case of highly tilted specimens, a detector at low take-off angle is mainly used. This technique was pioneered by McMullan (1953) with electron multipliers. Wells (1970) obtained good resolution of BSE images with a scintillation detector and found that in such configuration contrast originates in a shallow surface layer of the specimen. Even better results were obtained when only BSE with an energy close to the energy of primaries were collected (Wells, 1971). This low-loss technique needs BSE energy filter at the entrance of the detector. Wells *et al.* (1973) applied this technique to the microscope with a condenser-objective lens and with the detector placed below the lens, and Wells *et al.* (1990) placed the detector in the gap of the lens to make use of filtration properties of the lens. In the case of a detector at the higher position, the topographic contrast is reduced (Wells, 1978) and such a position can find use for detection of magnetic contrast.

Usually detectors give a mixture of topographic and material contrast with increasing amount of topographic contrast when the take-off angle decreases. In order to separate topographic contrast, detection systems containing two or more detectors were built. The topographic contribution in the signal depends strongly on the position of the detector, the material contribution much less. In the difference signal of two detectors, the material contribution is suppressed, and such a signal contains mainly topographic contrast. The detection systems were used for qualitative and quantitative assessment of the surface topography. They can be divided into two categories: symmetric and asymmetric ones (Fig. 6). Symmetric systems can be used for qualitative and quantitative work, asymmetric systems for qualitative work

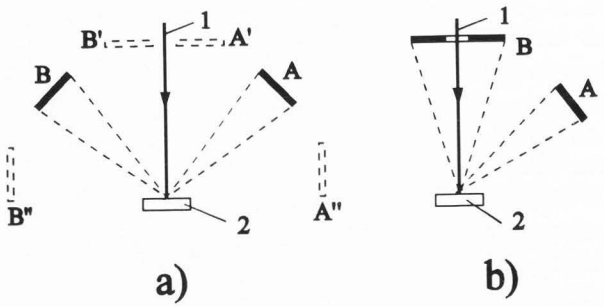

Figure 6. Positions of electron detectors in detector systems. (**a**) Symmetrical arrangements, A and B: detectors at medium positions (most often), A' and B': detectors at high positions, A" and B": detectors at low positions; (**b**) Asymmetrical arrangements, A: side detector, B: top detector. 1: primary beam, 2: specimen.

---

only. In symmetric arrangements, one pair or two pairs of detectors can be placed at medium (most often), high or low take-off angles. One pair of detectors is sensitive to the surface topography only in one direction; two pairs are sensitive in two directions (along X and Y axes). The first such systems was that of Kimoto *et al.* (1965) (Fig. 5a). Also the split detectors of Griffiths *et al.* (1972) and Munden *et al.* (1973) (Fig. 5c) as well as the MFD of Kuypers and Lichtenegger (1980) (Fig. 5j) can be used for a separation of the topographic contrast. Other systems are shown in Figure 7 (left: symmetrical arrangements, right: asymmetrical). Two pairs of semiconductor detectors were used by Lebiedzik (1979) (Fig. 7a) for quantitative surface reconstruction in X and Y directions. Volbert and Reimer (1980) used a pair of SE detectors (Fig. 7b); a converter plate was incorporated in this design, and it also allowed working with BSE. Reimer and Riepenhausen (1985) reported a system with a pair of pivoting SE detectors (Fig. 7c) which could be positioned in X and Y directions. Hejna and Reimer (1987) used a system with four scintillators at low take-off angles and with an additional top detector (Fig. 7d).

A pair of asymmetrically placed detectors, one for SE and the other for BSE was used by Crewe and Lin (1976) (Fig. 7e) for suppression of material contrast of biological specimens. The same approach with the SE and BSE-MFD detectors was applied by Volbert (1982) for other materials. Volbert (1982) and Reimer and Volbert (1982) showed that such a signal mixing technique cancels pseudo-topographic contrast of phase boundaries on flat specimens; this contrast appears when mixing techniques with BSE signals are used. Hejna *et al.* (1985) used an arrangement with a converter as one detector and semiconductors diodes as the second detector (Fig. 7f). A similar design with the ring detector instead of the converter was used by Buczkowski *et al.*

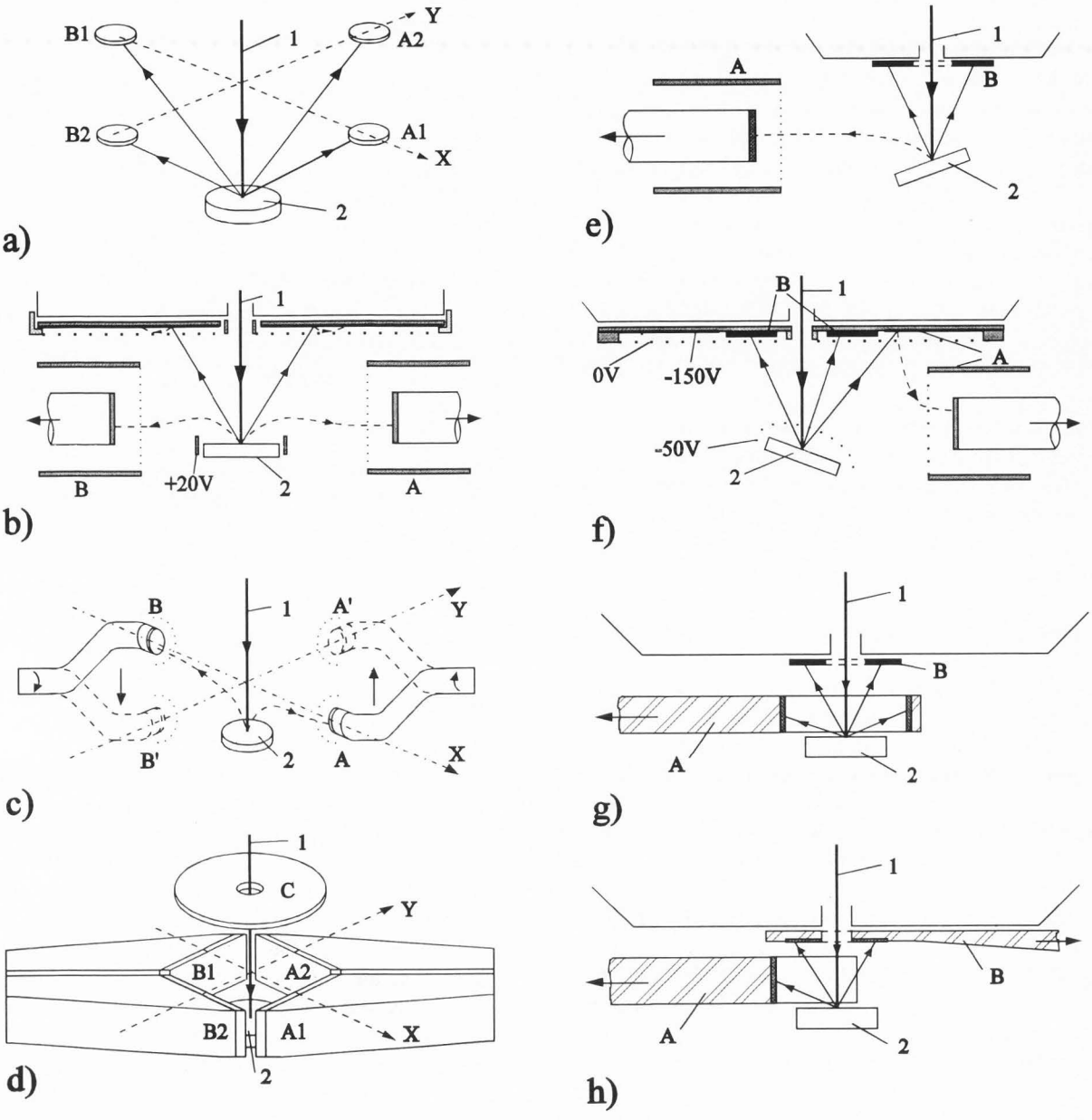

Figure 7. Detector systems used for obtaining topographic contrast. Left panel: symmetrical arrangements; right panel: asymmetrical arrangements. (**a**) Pairs of semiconductor or scintillation BSE detectors (A1-B1 and A2-B2) (two pairs as in Fig. 7a or one pair only); (**b**) two E-T detectors for SE (A and B) with the converter plate for suppression of SE3, the system can be used also for BSE in conversion mode; (**c**) a pair of pivoting SE detectors (A and B in one position and A'-B' after pivoting to second position) (an alteration of the system from Fig. 7b); (**d**) two pairs of low take-off scintillation detectors (A1-B1 and A2-B2) and top detector (C), all detectors for BSE; (**e**) E-T detector for SE (A) and top detector for BSE (B); (**e**) converter (ETD plus converter plate) as detector A and semiconductor diodes as detector B; (**f**) ring detector (A) and top detector (B); (**g**) sector-shaped ring detector (A) and top detector (B); and (**h**) shows a variation of arrangement in Figure 7g with a sector-shaped ring detector and a scintillation top detector. 1: primary beam, 2: specimen.

(1988) (Fig. 7g). They showed that this arrangement reduces pseudo-topographic contrast in comparison to symmetric arrangements of BSE detectors. Figure 7h shows a variation of this arrangement with a sector-shaped ring detector and a scintillation top detector.

Methods of Testing Detectors and Detector Systems

Knowledge of performances of different detectors and detector systems can help us in choosing an appropriate detector or detector system for particular application. Characteristics of detectors and detector systems can be predicted theoretically or tested experimentally.

Tilt contrast of a particular detector or a detector system can be calculated by integrating the formulas describing the distribution of emitted electrons in a solid angle of detection (Reimer *et al.*, 1984) or by integrating experimental values of a signal distribution, $dS/d\Omega$, measured with a small BSE detector (Reimer and Riepenhausen, 1985). Experimentally, it can be checked by recording the image of a ball, a specimen which contains all tilt angles from 0° to 90° at all azimuths with respect to the detector. Blaschke and Schur (1974) recorded linescans across a ball at different detector take-off angles, Lange *et al.* (1984) recorded iso-densities for several detectors and detector systems.

Electron detectors do not collect all electrons emitted from the specimen surface. SE are attracted by a positive potential of the detector and only part of the SE reaches the detector. The amount of collected electrons depends on the electric field distribution in the specimen chamber; that is a function of the geometry of the chamber interior. The field distribution depends on the design of the SE detector and on the presence of other detectors at the specimen, on the working distance, and on the tilt and the shape of the specimen. An influence of the first two factors on SE tilt contrast obtained with two different SE detectors, showed in Figure 8, is demonstrated in Figure 9. The linescan recorded with the detector from Figure 8a, without BSE detectors at the specimen, is typical for SE tilt contrast (Fig. 9a), but it changes when BSE detectors are placed at the specimen (Figs. 9b and 9c). SE tilt contrast obtained with the detector from Figure 8b is influenced very little by BSE detectors (Figs. 9d and 9e). Generally, SE tilt contrast is not reproducible when any of the factors mentioned earlier are changed. BSE travel along straight lines, and that part which is emitted into a solid angle subtended by the detector is collected. However, electrons can be transferred into a signal with different efficiency depending on the place where they strike the detector. The distribution of the detection efficiency over a surface of the BSE detector can be checked with a primary beam reflected from an electrostatic mirror. Brunner (1983) used a charged teflon plate and a biased metal electrode for this purpose; Alvarez *et al.* (1984) used a charged glass ball, and Autrata and Hejna (1991) a biased metal ball. The scanned primary beam is reflected in a mirror field and scans the interior of the microscope chamber and also the BSE detectors. On the screen, we obtain a

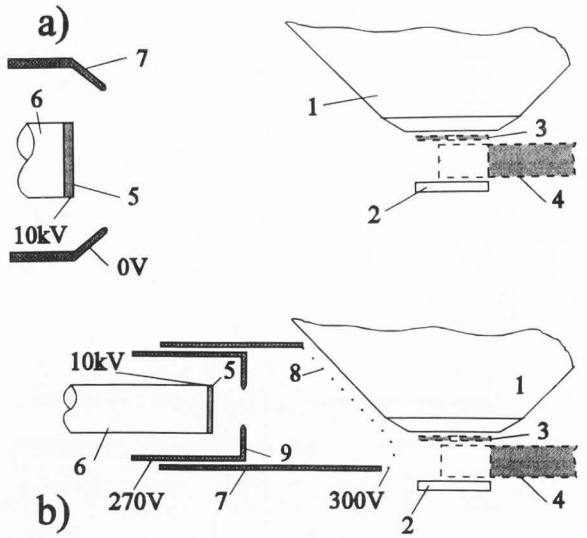

Figure 8. SE detectors used for recording images in Figure 9. (**a**) Detector without entrance grid, placed far from the specimen, (**b**) detector with biased entrance grid, placed close to the specimen. 1: microscope lens; 2: specimen; 3: top BSE detector (if present); 4: sector-shaped ring BSE detector (if present); 5: scintillator; 6: light-guide; in Figure (a), 7: shielding tube around scintillator; in Figure (b), 7: outer tube; 8: entrance grid; 9: aperture.

---

distribution of the signal strength over the detector surface. Semiconductor detectors have uniform detector efficiency. Scintillation detectors show usually non-uniform efficiency because light-guides do not transport the light with equal efficiency from different places on the detector surface. Converters also show non-uniform efficiency because the SE detector collects more electrons generated in its proximity.

The response of the detector to material contrast can be studied experimentally by preparing a calibration curve (signal versus atomic number Z) for a given detector and experimental conditions (Ball and McCartney, 1981).

Topographic contrast of edges and small features can be studied theoretically and experimentally by computing and recording linescans across them. The number of features of different shape is unlimited and tests are applied to some features of simple geometry: steps, bars, grooves, balls, etc. The edge effect was investigated by Christenhuss and Reimer (1969) for SE and BSE. George and Robinson (1975) studied theoretically (with a simple Monte-Carlo technique) and experimentally, the contrast of small cubes on the flat surface; George and Robinson (1977) computed signals of other features (double steps, ripples). Hasselbach and Rieke (1976) investigated emission of SE at edges with an emission microscope and found that SE can be generated

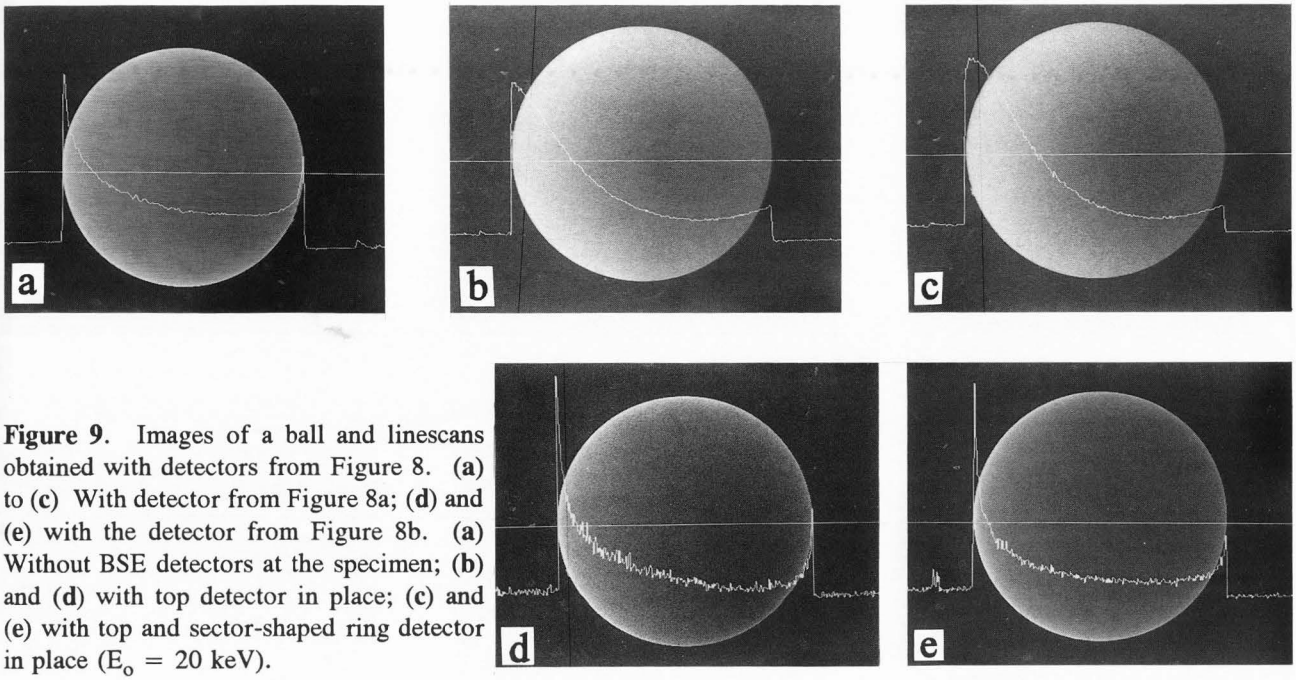

Figure 9. Images of a ball and linescans obtained with detectors from Figure 8. (**a**) to (**c**) With detector from Figure 8a; (**d**) and (**e**) with the detector from Figure 8b. (**a**) Without BSE detectors at the specimen; (**b**) and (**d**) with top detector in place; (**c**) and (**e**) with top and sector-shaped ring detector in place (E_o = 20 keV).

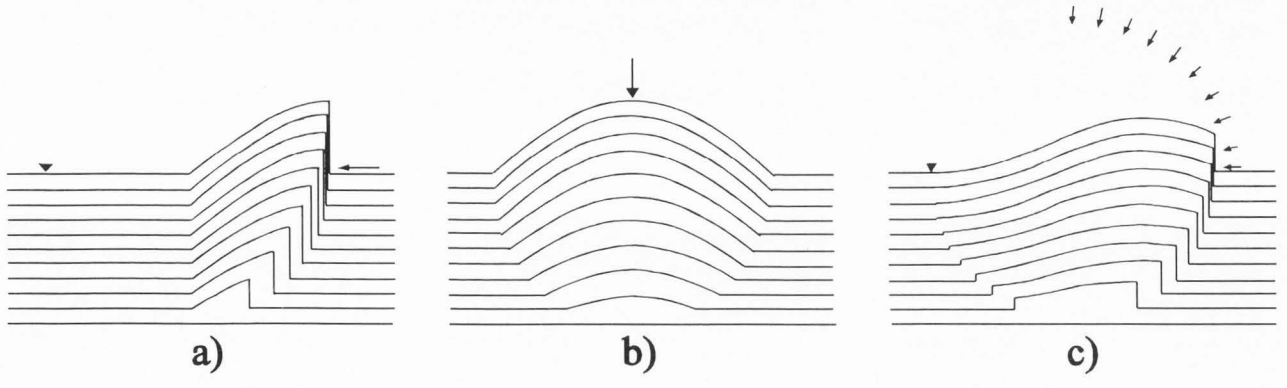

Figure 10. Computed signals of the light intensity scattered from the ball (Reimer *et al.*, 1984). (**a**) Ball illuminated from one side, (**b**) from the top, and (**c**) from the right half of the upper hemisphere. Arrows show direction of light beams and triangle indicates left edge of the ball.

---

by BSE far from the primary beam. Linescans for different features (steps, bars, grooves), used as an alignment marks in electron lithography, were studied experimentally and theoretically by many authors, e.g., Stephani (1979) with Monte-Carlo technique, Shiraki and Aizaki (1981) with very simple and Czyzewski and Kaczmarek (1985) with more complex analytical models. Reimer *et al.* (1986) recorded BSE signals from edges and steps at different detector take-off angles. Reimer and Stelter (1987) computed, by Monte-Carlo method, signals for surface steps. A dependence of a signal of small ripples on take-off angle of detection was investigated experimentally by Hejna (1988). SE and BSE signals of multiple photoresist bars on a Cr-coated Si-wafer were studied by Endruschat *et al.* (1989). Desai and Reimer (1990) and Czyzewski and Joy (1991) used Monte-Carlo techniques for calculating diffusion matrices for electron scattering and applied them for fast calculation of linescans across steps for BSE and SE, respectively. Kotera *et al.* (1990) did detailed Monte Carlo calculations for SE profiles of bars.

Material contrast of small features can also be computed theoretically or recorded experimentally for selected features. Robinson and George (1976) studied experimentally and theoretically material contrast of small cubes and slices of one material in another. DeNee (1978) investigated a signal of small spherical particles of a heavy element on a light element substrate. Rosenfield *et al.* (1983) studied theoretically and experimentally the contrast of gold bars on a Si substrate.

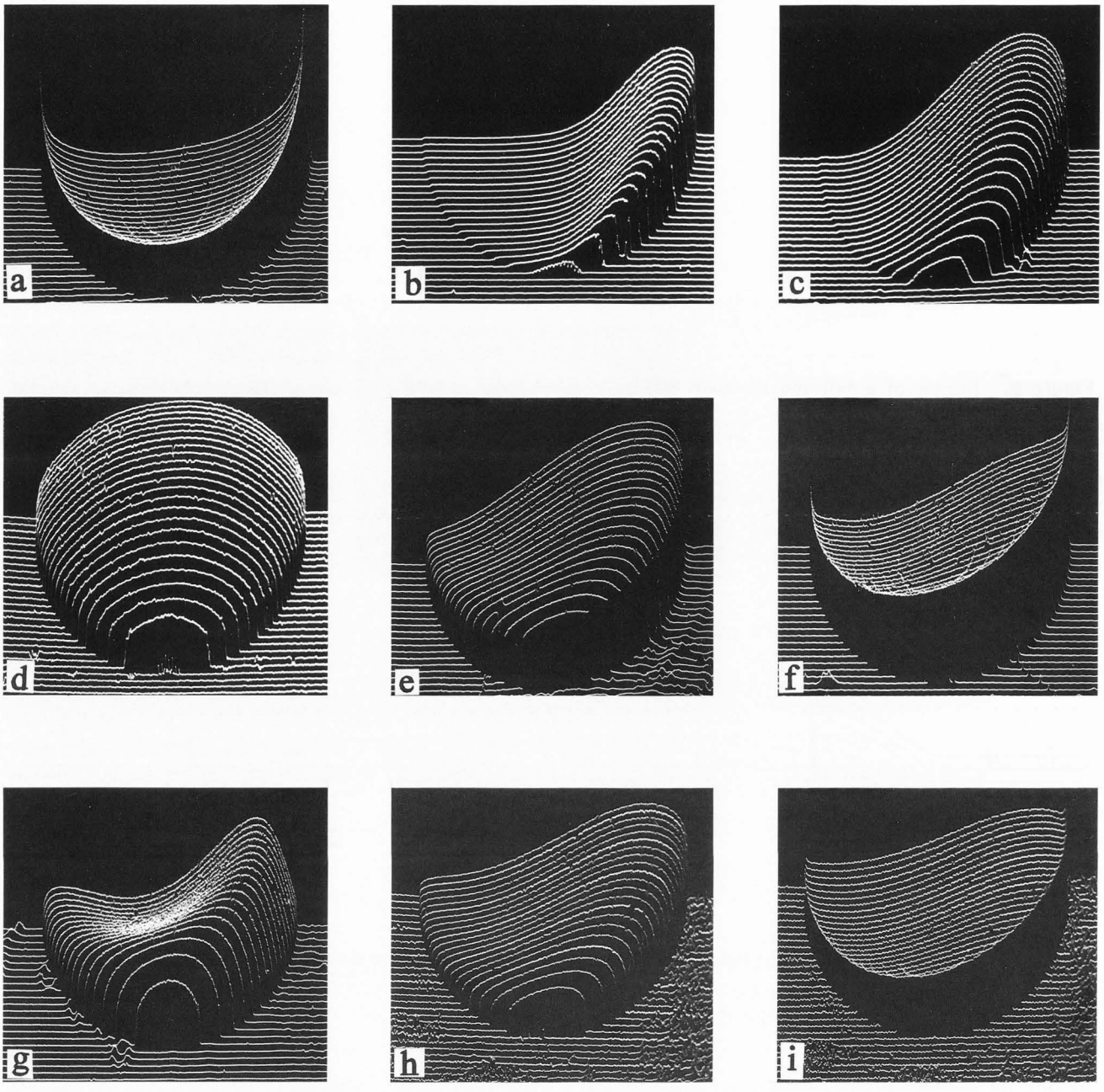

Figure 11. Recorded electron signals from 1 mm steel ball specimen. (**a**) SE signal of ETD, (**b**) BSE signal of ETD, (**c**) BSE signal of large area side detector, (**d**) BSE signal of top detector, (**e**) BSE signal of converter, (**f**) (BSE + SE) signal of converter, (**g**) BSE signal of ring detector, (**h**) BSE signal of sector-shaped ring detector, (**i**) sum of BSE signal of sector-shaped ring detector and SE signal of ETD. E_o = 20 keV.

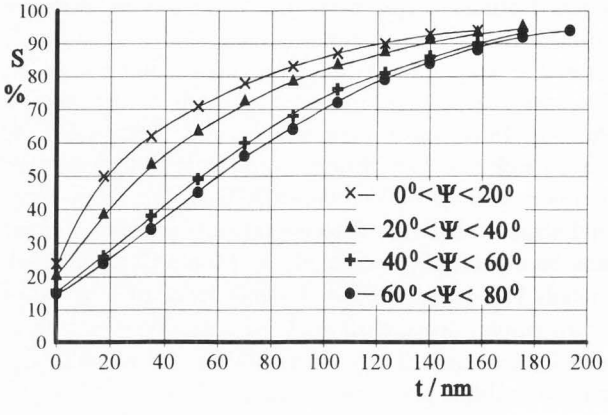

Figure 12. Dependence of the signal of BSE scintillation detector on Au layer thickness (as a percentage of a signal from thick Au) for different ranges of take-off angles Ψ. Specimen: Au layer on Si substrate. E_o = 20 keV.

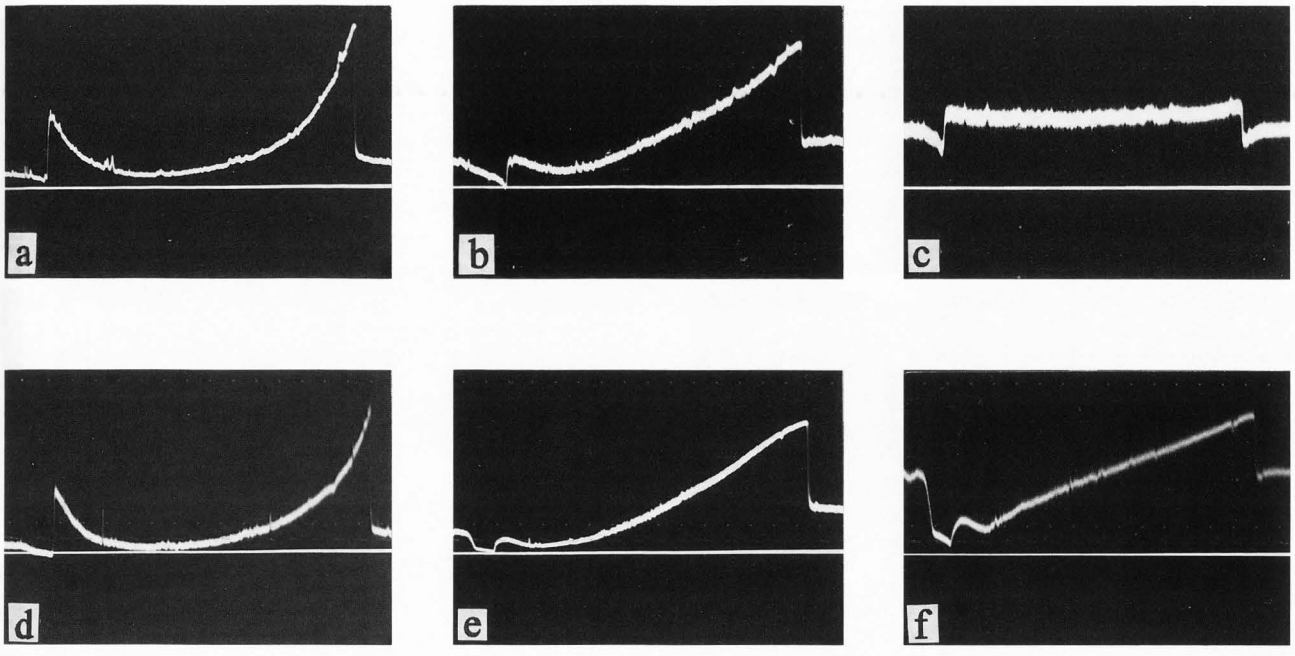

Figure 13. Linescans across 1 mm hemisphere of polyvinyl alcohol covered with a 20 nm layer of gold. (**a**) to (**c**) Uniformly sputter-coated, and (**d**) to (**f**) unidirectionally evaporated at an angle of 45° and additionally uniformly evaporated with carbon. (**a**) and (**d**) SE signals of ETD, (**b**) and (**e**) BSE signals of sector-shaped ring detector, and (**c**) and (**f**) BSE signals of top scintillation detector. E_0 = 20 keV.

Radzimski and Russ (1989) studied sharpness of edges for layers buried in a matrix of another element for BSE of different energies. Aristov *et al.* (1991) developed an analytical model for the contrast of micro-inhomogeneities buried at different depths under the surface.

Performances of Detectors and Detector Systems

The best perception of the tilt contrast occurs when it is similar in appearance to the contrast of objects illuminated by light, known from our surrounding world. Generally, this is not the case in SEM micrographs. Reimer *et al.* (1984) computed signals for a ball illuminated with light and showed signals in the form of Y-modulated images (Fig. 10). The best perception of the tilt contrast occurs for diffuse illumination from one side (Fig. 10c) (the whole surface is imaged, the signal is a monotone function of tilt and directionality of the signal makes interpretation of the shape easier). Topographic contrast of a specimen of uniform composition differs from that of a specimen covered with a layer of other material, and both cases are discussed separately.

Figure 11 shows experimentally recorded Y-modulation images of the lower half of a uniform metal ball obtained with some of the detectors discussed above. The secondary electron signal (Fig. 11a) has no analogy in light illumination and this fact is a drawback of SE as used for topographic contrast. Good tilt contrast can be obtained with BSE signals of a converter and a sector-shaped ring BSE detector (Figs. 11e and 11h), and it can be even better when we add some amount of the SE signal to the BSE signal (Figs. 11f and 11i). In the case of a converter, this is realized by detection of SE and converted BSE with the same detector, and, in the case of a sector-shaped ring detector it is realized by adding a signal of an SE detector electronically. Insulating specimens need to be covered with thin conductive layers. Coating of a specimen of low atomic number with a layer of a high Z material also increases the signal strength and improves the resolution (Ong, 1970). The BSE coefficient η increases at first linearly with increasing layer thickness; next, the slope decreases and η saturates at the layer thickness of about R/2 (Cosslett and Thomas, 1965; Hohn *et al.*, 1976; Niedrig, 1982). Similar dependence on the layer thickness was also found for the signal of the wide-angle scintillation top detector (Rajora and Curzon, 1985). Measurements of BSE signals at various ranges of take-off angles Ψ (Figure 12) indicate that the dependence of the signal on layer thickness varies with the take-off angle of the detector. Measurements for Au layers on Si substrate were made with an annular top detector (ranges 40°-60° and 60°-80°) and with a ring detector (ranges 0°-20° and 20°-40°). The signal of the low take-off detector increases much faster than that of the high take-off detector when the layer thickness starts to increase from zero value. In a low resolution case, the thickness of the layer is 10-30 nm, and its uniformity depends on the method of coating.

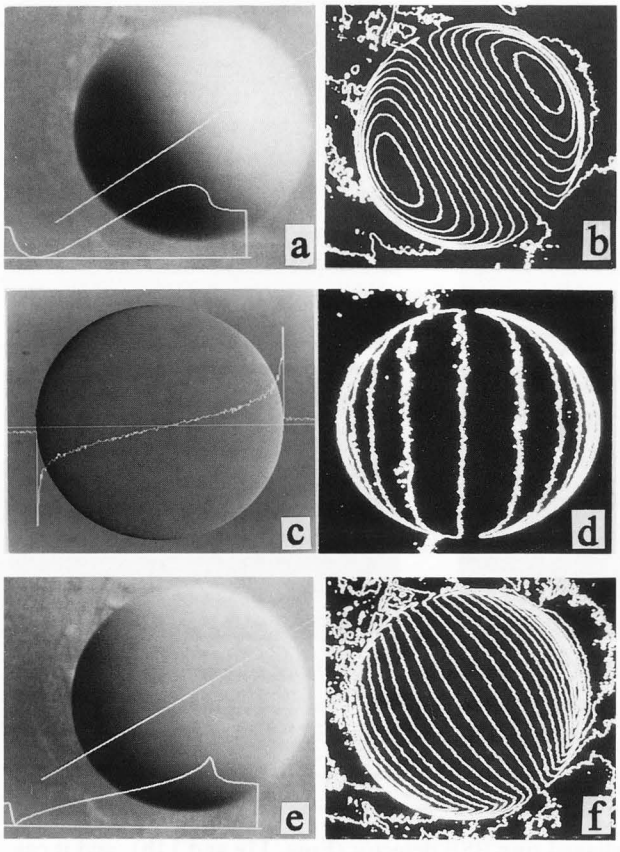

Figure 14 (at left). Images with linescans of a ball (left) and iso-densities (right) for different symmetrical detector systems. (**a**) and (**b**) (S_A-S_B) signal of a pair of BSE detectors, (**c**) and (**d**) (S_A-S_B) signal of a pair of SE detectors, (**e**) and (**f**) (S_A-S_B)/S_C signal of a system from Figure 7d. E_o = 20 keV.

Note: Figure 16 is on facing page 155.

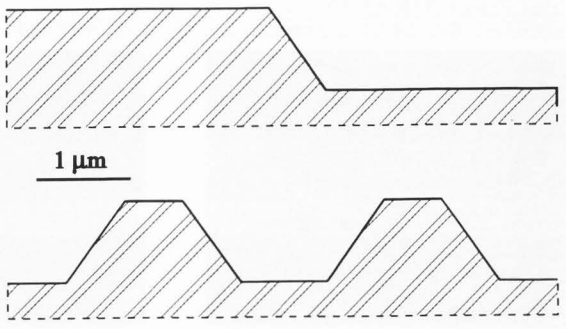

Figure 17. Cross-sections of a step and multiple bars etched in a Si wafer, used for the recording of linescans in Figures 18 and 19 (facing page).

The layer thickness is highly non-uniform for unidirectional evaporation and more uniform when the specimen is pivoted and rotated during evaporation and also for sputter coating. Figures 13a-13c show linescans across a hemisphere made of polyvinyl alcohol and sputter-coated with 20 nm of gold. The tilt contrast of SE is similar to that of a uniform specimen, a top detector for BSE does not give contrast on a sphere, and only some shadowing effect can be seen outside the sphere, and a sector-shaped ring BSE detector gives a good tilt contrast. Figures 13d-13f show linescans across a hemisphere unidirectionally evaporated with gold (at an angle of 45°) and, additionally, with a uniform layer of carbon. The linescans from SE detector and sector-shaped ring BSE detector are similar to those in Figures 13a and 13b; the linescan for the top BSE detector shows a thickness contrast, which can be used for imaging the topography.

The detection systems used for the suppression of the material contribution in the topographic contrast differ in their sensitivity to the surface tilt. Figure 14 shows images of a metal ball with linescans and iso-densities for symmetrical systems. The signal in Figure 14a is proportional to the sine, that in Figure 14c to the tangent of a tilt angle, and that in Figure 14e directly to the tilt angle. Figure 15 shows images with linescans for asymmetrical systems. Signals of systems using SE are more sensitive to large tilt angles, and those using BSE have more uniform dependence of the signal on the tilt angle.

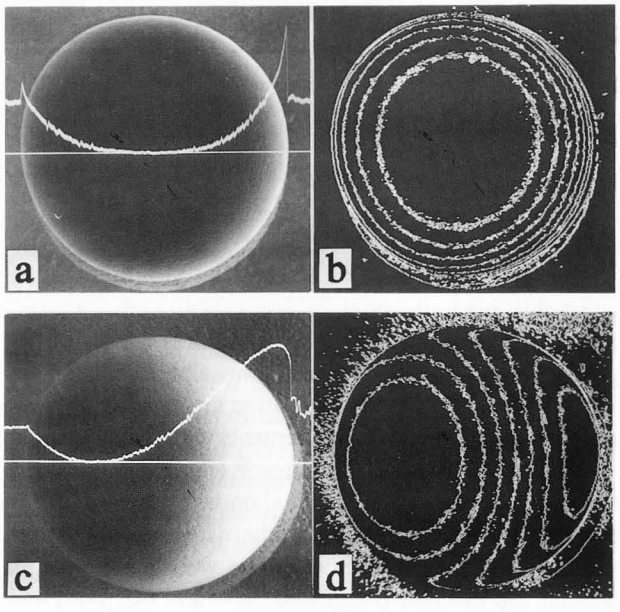

Figure 15. Images with linescans of a ball (left) and iso-densities (right) for different asymmetrical detector systems. (**a**) and (**b**) Difference signal of SE detector and BSE top detector, and (**c**) and (**d**) difference signal of sector-shaped ring and top BSE detectors. E_0 = 20 keV.

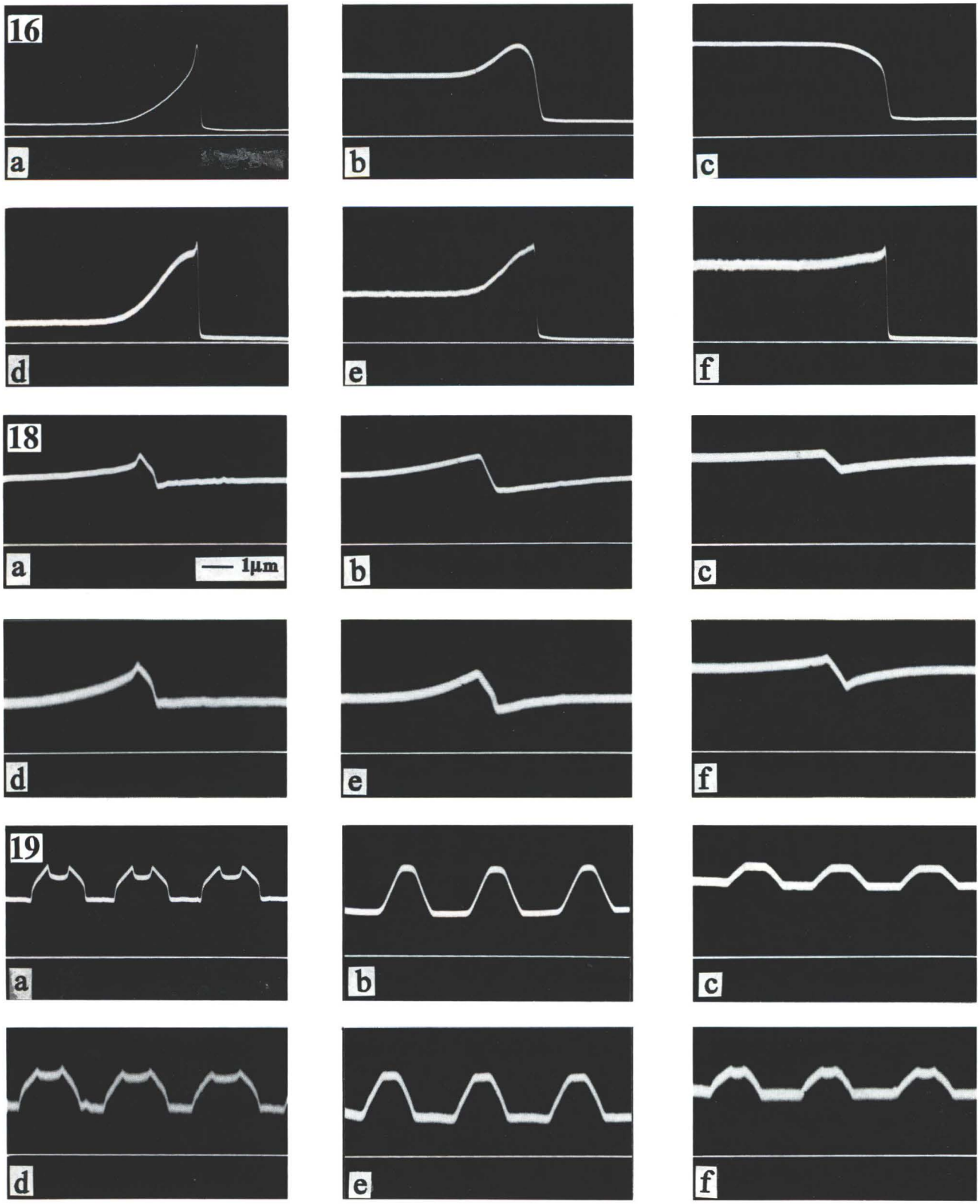

Figures 16, 18 and 19. Linescans: across an edge of a Si wafer (edge contrast), E_o = 20 keV (**Figure 16**); across a step (**Figure 18**), and across multiple bars (**Figure 19**) shown in Figure 17; E_o = 30 keV. (**a**) to (**c**) uncoated specimens, and (**d**) to (**f**) gold coated specimens; (**a**) and (**d**) SE detector, (**b**) and (**e**) sector-shaped ring BSE detector, and (**c**) and (**f**) top BSE detector.

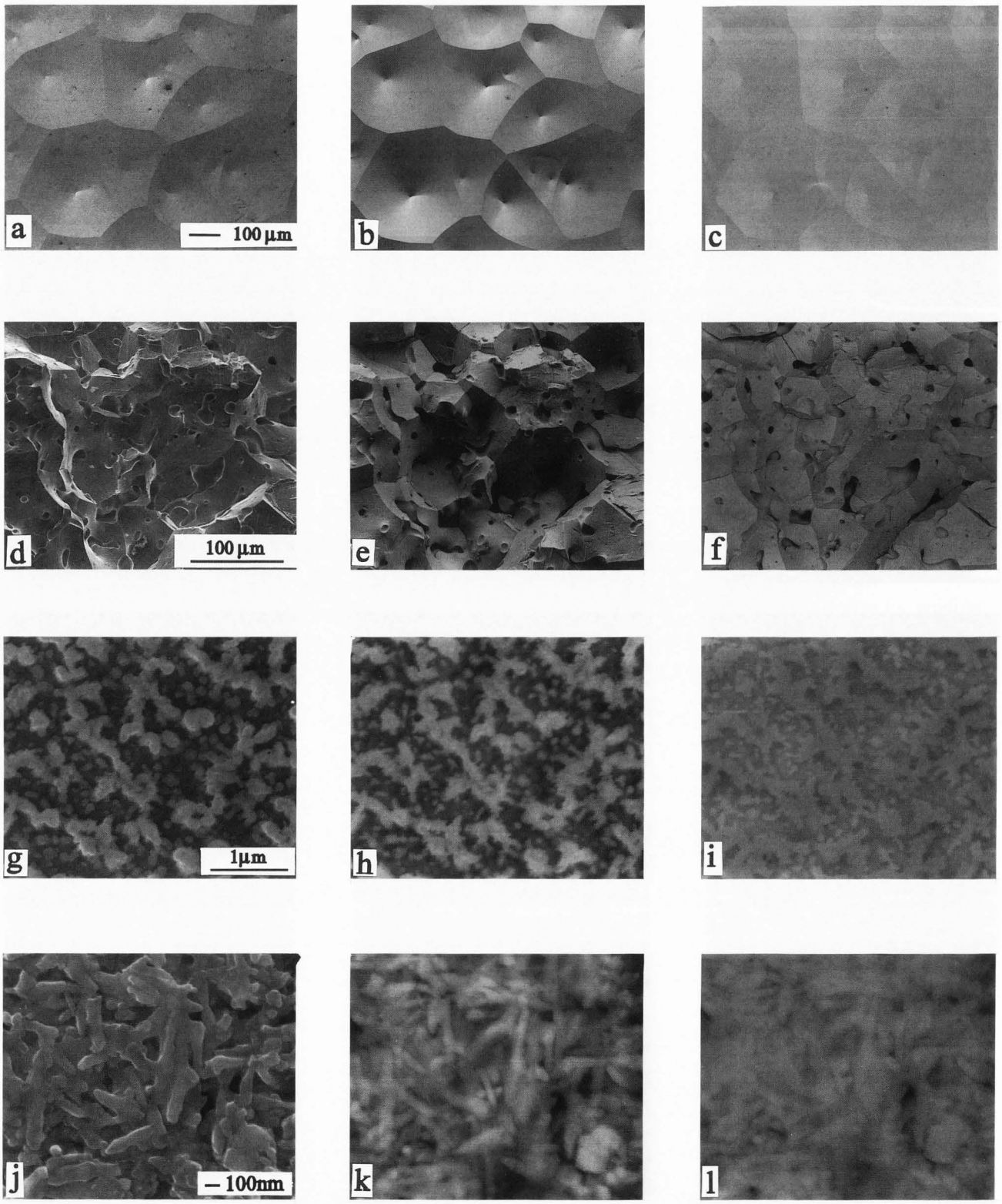

Figure 20. Images of specimens of uniform composition obtained with different detectors. Left panel: with SE detector, middle panel: with sector-shaped ring BSE detector, right panel: with top BSE detector. (**a**) to (**c**) Etched cobalt specimen, (**d**) to (**f**) fracture of sintered iron, (**g**) to (**i**) plasma etched gold layer, and (**j**) to (**l**) surface of magnetic floppy disc. E_o = 20 keV.

Figure 21. Images of an iron grain obtained with different modes of a converter. (**a**) SE image, (**b**) BSE image, and (**c**) (BSE+SE) image. E_o = 20 keV.

Figure 16 shows an edge effect for three detectors: E-T detector for SE, sector-shaped ring and top detectors for BSE. The specimen is a cleaved Si wafer, uncoated (Figs. 16a-16c) and sputter coated with a 20 nm layer of gold (Figs. 16d-16f). The edge effect is very strong for SE (Figs. 16a and 16d). When the beam strikes a specimen close to an edge, there is a large amount of forward-scattered BSE which leave the side surface of the specimen and generate SE. The forward-scattered BSE do not contribute to signals of both BSE detectors, but SE generated by them contribute to the signal of the ETD. As a result, there is a peak of the SE signal at the edge and low BSE signals. When the beam moves from the edge, the amount of forward-scattered BSE decreases, and an increasing number of BSE is emitted from the side surface in a backward direction, mainly to low take-off angles [wide peak in the low take-off BSE signal (Figure 16b) and corresponding long tail in the SE signal (Figure 16a)]. When BSE cannot leave the side surface they all undergo full scattering processes and a larger number of them is scattered to high take-off angles (saturation of the signal in Figure 16c). Gold coating of the specimen increases the scattering in the surface layer and improves the edge sharpness in BSE modes (Figs. 16e and 16f). In the SE mode (Figure 16d), we notice the absence of the peak from forward BSE, a larger tail caused by low take-off BSE and a small peak caused by high take-off BSE as a result of an increase of the layer thickness at an edge. To decrease an edge effect in the SE mode, Wells (1978) proposed special orientation of the specimen in respect to the detector; Wells and Bailey (1985) and Wells (1986) mounted a special control electrode between the specimen and the detector. Wells (1988) found that the edge effect is very low for the low-loss technique.

A large number of linescans for different surface features were published in papers referred in the previous section and in many other papers. An example of linescans for a step and a bar (drawn in Figure 17) are shown in Figures 18 and 19 for three detectors (the same as used for recording linescans in Figure 16). Linescans in Figures 18a-18c and 19a-19c are from uncoated specimens and those in Figures 18d-18f and 19d-19f from gold coated specimen. Gold coating modifies the SE signal only very little and improves the edge sharpness for high take-off BSE. Linescans were recorded at different locations on the wafer and only the shape of the signals but not their geometrical dimensions can be compared.

Applications

In this section, micrographs of different specimens imaged with different detectors are shown to demonstrate how the choice of the detector influences the appearance of an image.

Figure 20 shows images of uniform specimens obtained with the ETD for SE (left panel), the sector-shaped ring BSE detector (middle panel), and the top BSE detector (right panel) for BSE. The sector-shaped ring BSE detector gives a high level of tilt contrast and a good three-dimensional impression of the specimen shape (Figs. 20b and 20e). The SE image of a rough specimen (Fig. 20d) looks relatively flat with high contrast of the edges and small features. The image of the top detector (Fig. 20f) is not directional, and this fact can lead to a wrong interpretation of the specimen shape. Comparing the scattering contrast of small features in Figs. 20g-20l, we see that it decreases in the BSE modes when features become small comparable with an electron range (Figs. 20k and 20l in comparison to Figs. 20h and 20i), and it is larger for the sector-shaped ring detector than for the top detector. As was mentioned earlier, the sum of the BSE signal of the converter or the sector-shaped ring detector and the SE signal gives good tilt contrast and good edge sharpness. This is demonstrated on images of an iron grain in Fig. 21. The SE image shows a flat grain with very rough surface, the BSE image shows a good shape of the grain and the (BSE + SE) image shows good shape and good sharpness of surface features.

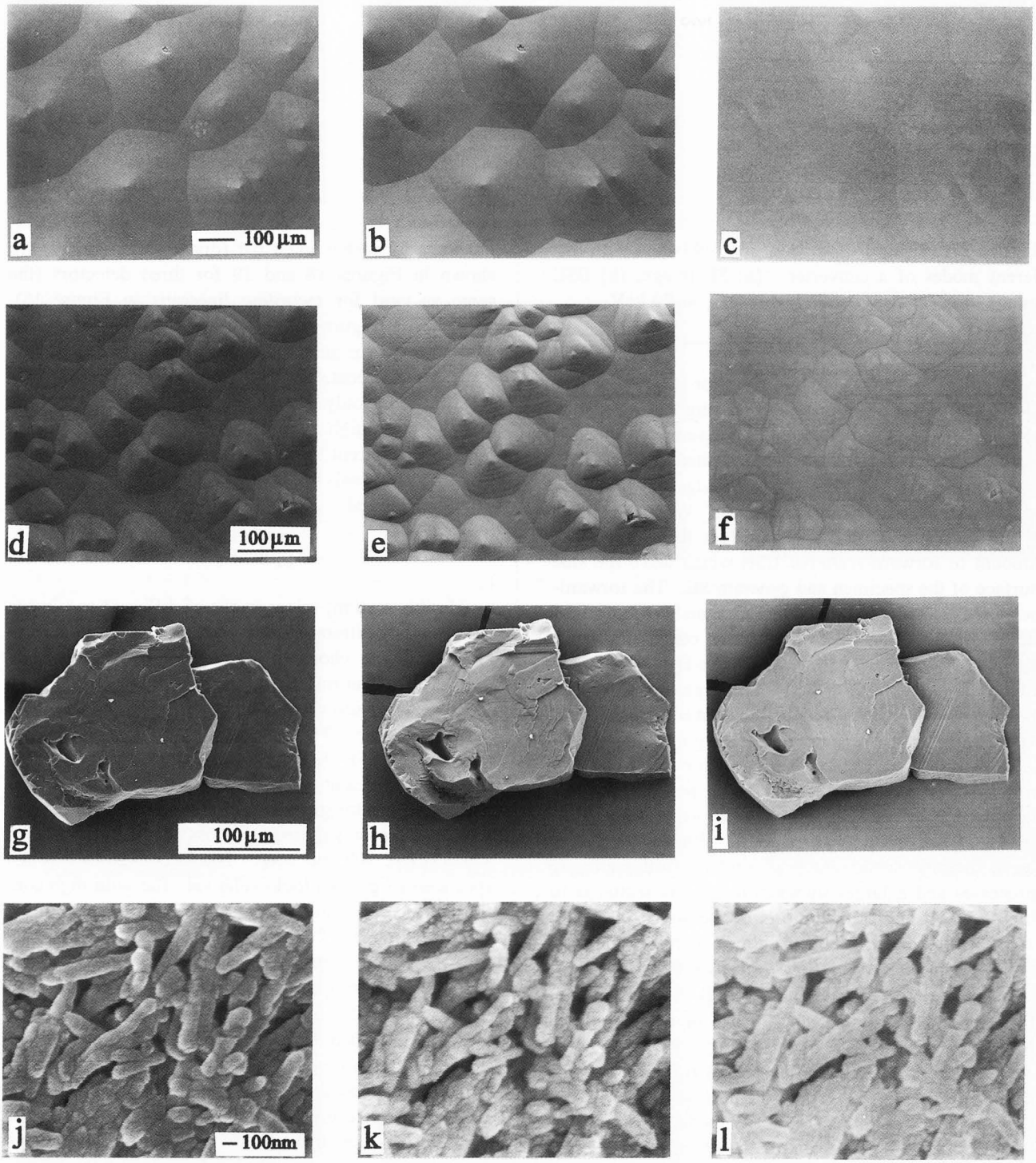

Figure 22. Images of gold coated specimens obtained with different detectors. Left panel: with SE detector, middle panel: with sector-shaped ring BSE detector, right panel: with top BSE detector. (**a**) to (**c**) plastic replica of etched cobalt specimen, (**d**) to (**f**) plastic replica of etched GaAs wafer, (**g**) to (**i**) synthetic diamond, and (**j**) to (**l**) magnetic tape. E_o = 20 keV.

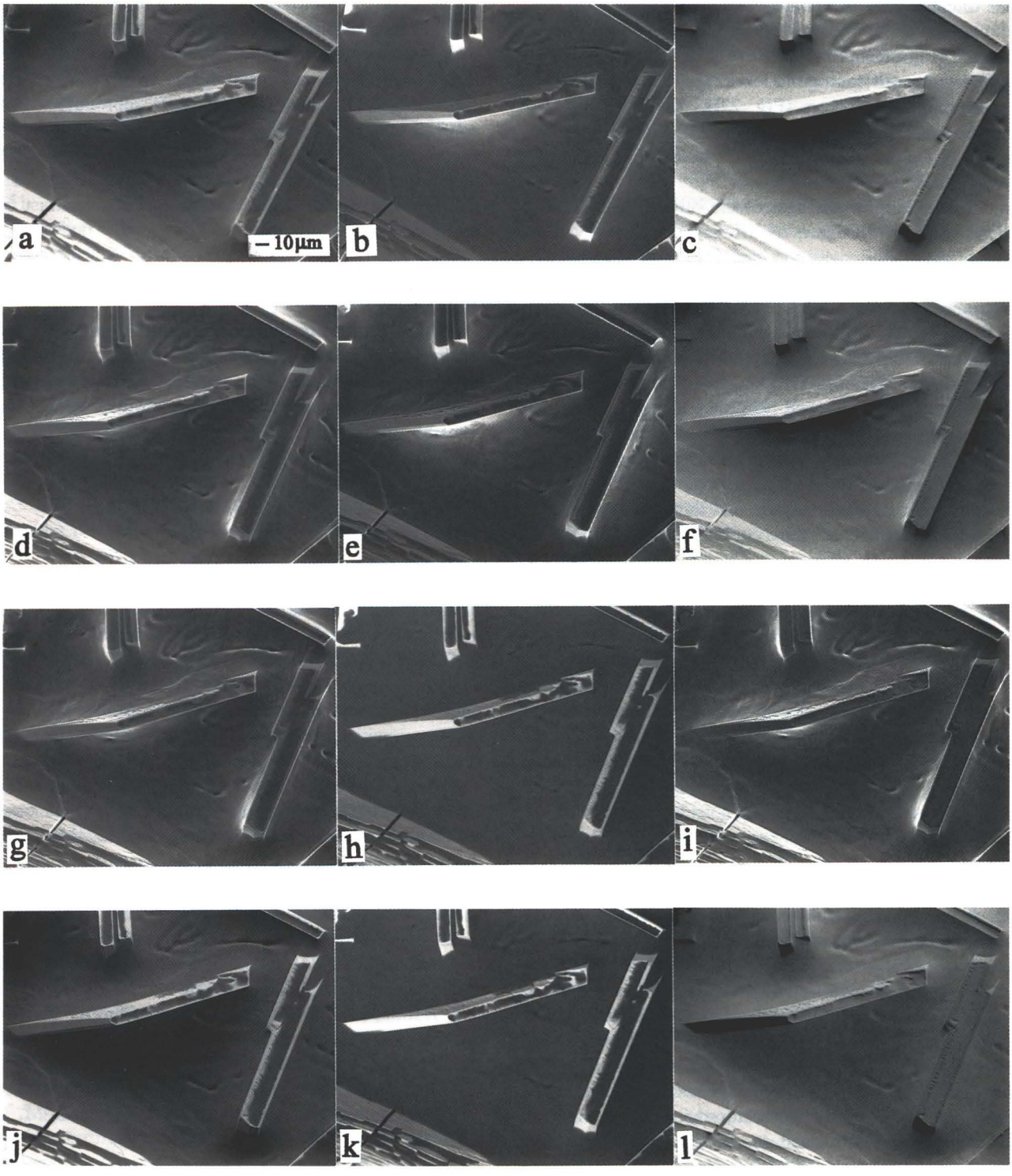

Figure 23. Images of an Al-W alloy obtained with different two-detector systems. Left panel: topographic images obtained with first detector, middle panel: images obtained with second detector, right panel (**c**, **f**, **i**, and **l**): topographic images obtained with difference signal of first and second detectors. (**a**) and (**b**) BSE images (obtained by conversion at lens pole-piece), (**d**) and (**e**) SE images, (**g**) and (**h**) SE image and BSE image of top detector, and (**j**) and (**k**) BSE images of sector-shaped ring and top detector. E_o = 20 keV.

In the case of gold coated specimens (Fig. 22), good tilt contrast is obtained with the sector-shaped ring BSE detector (Figs. 22b, 22e and 22h). For the high take-off BSE detector tilt contrast is low (Figs. 22c and f), and an edge contrast appears (Fig. 22i). Gold coating increases scattering of electrons and improves scattering contrast of small features in BSE modes (Figs. 22k and 22l).

Figure 23 shows images of the surface of an Al-W alloy obtained with signals of different electron detectors and topographic images obtained with mixed signals of different detector systems. The BSE (S_A-S_B) image of a symmetrical arrangement of two high take-off BSE detectors (Fig. 23c) is the most diffuse in appearance. The detection of BSE was done by conversion to SE at the lens polepiece. The BSE (S_A-S_B) image of an asymmetrical arrangement of a low take-off and a high take-off detector is less diffuse (Fig. 23l). The detectors were a sector-shaped ring detector and an annular top scintillation detector. The (S_{SE}-k^*S_{BSE}) image (Fig. 23i) shows good contrast of small features and thin dendritic structures on the surface, but edge contrast is very strong and three-dimensional impression of larger crystals is worse than in BSE images. In the SE (S_A-S_B) mode (Fig. 23f), contrast of the majority of small surface features cancels, and the resulting image is very similar to BSE images.

Signals of symmetrical systems can be used for quantitative reconstruction of surfaces. This problem was investigated, e.g., by Lebiedzik (1979), Niemietz *et al.* (1984) and Carlsen (1985). Surface reconstruction from a signal of one BSE detector was proposed by Frisova *et al.* (1991).

Conclusions

In low-resolution, low-magnification SEM images, topographic tilt contrast dominates. SE signal does not give a good, reproducible contrast. From a variety of BSE detectors, converter and sector-shaped ring detectors give good topographic tilt contrast. Poor sharpness of edges in BSE images in comparison to SE images can be improved by adding some amount of a SE signal to a BSE signal. In the case of specimens coated with thin layers of heavy metals, the sector-shaped ring detector gives good tilt contrast and good edge sharpness.

At medium resolution, diffusion contrast of features smaller than an interaction volume of primary electrons dominates. The SE signal gives sharp images with bright edges of features. BSE signals give more diffuse images, especially in the case of low-density materials, and contrast is higher for a low take-off detector. In the case of coated specimens, the SE detector and the sector-shaped ring BSE detector give sharp images with a high contrast.

In the case of specimens of non-uniform composition, detector systems are used for suppression of the material contribution in the signal. Detector systems containing BSE detectors give more reproducible tilt contrast with more uniform dependence of the signal on tilt angles than systems containing SE detectors. At medium resolution, the difference signal of the SE detector and the BSE detector gives good contrast of small topographic features.

Acknowledgments

Part of the work was done during the author's stay at the Institute of Physics of the University of Münster (Germany); the author is indebted to Professor L. Reimer for placing the laboratory at his disposal and for valuable discussions. The support of the stay by the Katholischer Akademischer Ausländer Dienst is also gratefully acknowledged.

References

Alvarez AG, Bonetto RD, Guerin DMA, Peez CG (1984) Images of the inner parts of scanning electron microscopes. Electr. Optics Bulletin **120**, 39-43.

Aristov W, Dreomova NN, Frisova AA, Kazmiruk VV, Samsonovich AV, Ushakov NG, Zaitsev SI (1991) Signal formation of backscattered electrons by micro-inhomogeneities and surface relief in a SEM. Scanning **13**, 15-22.

Arnal F, Verdier P, Vincensini PD (1969) Coefficient de retrodiffusion dans le cas d'electrons monocinetiques arrivant sur la cible sous une incidence oblique. (Backscatter coefficient in the case of monoenergetic electrons impinging on the sample at an acute angle). Compt. Rend. Acad. Sci. (Paris) **268**, 1526-1529.

Autrata R (1984) A double detector system for BSE and SE imaging. Scanning **6**, 174-182.

Autrata R (1990) A modification of the ET secondary electron detector with a single crystal scintillator. Scanning **12**, 119-125.

Autrata R, Schauer P, Kvapil J, Kvapil J (1978) A single crystal of YAG - new fast scintillator in SEM. J. Phys. **E 11**, 707-708.

Autrata R, Schauer P, Kvapil 1, Kvapil J (1983a) A single crystal of $YAlO_3$:Ce^{3+} as a fast scintillator in SEM. Scanning **5**, 91-96.

Autrata R, Schauer P, Kvapil J, Kvapil J (1983b) Single-crystal aluminates - a new generation of scintillators for scanning electron microscopes and transparent screens in electron optical devices. Scanning Electron Microsc. **1983**; II: 489-500.

Autrata R, Hejna J (1991) Detectors for low voltage scanning electron microscopy. Scanning **13**, 275-287.

Ball MD, McCartney DG (1981) The measurement of atomic number and composition in an SEM using backscattered detectors. J. Microsc. **124**, 57-68.

Baumann W, Reimer L (1981) Comparison of the noise of different electron detection systems using scintillator-photomultiplier combination. Scanning **4**, 141-151.

Bishop HE (1966) Some electron backscattering measurements for solid targets. In: Proc. 4th Int. Congr. X-Ray Opt. Microanal. Hermann, Paris. 153-158.

Blaschke R, Schur K (1974) Der Informationgehalt des Rückstreubildes im Rasterelektronenmikroskop (Information content of the backscatter image in the scanning electron microscope). BEDO **7**, 33-52.

Boyde A, Cowham MJ (1980) An alternative method for obtaining converted back-scattered electron images and other uses for specimen biasing in biological SEM. Scanning Electron Microsc. **1980**; I: 227-232.

Brunner M (1983) Simulation of backscattered electrons by reflection of primary electrons applied to optimization of detector designs. Appl. Phys. Lett. **43**, 391-393.

Buczkowski A, Hejna J, Radzimski Z (1988) Signal mixing technique for backscattered electrons in the scanning electron microscope. Scanning Microsc. **2**, 633-638.

Carlsen IC (1985) Reconstruction of true surface topographies in scanning electron microscopes using backscattered electrons. Scanning **7**, 169-177.

Chang THP (1974) Detection of electron signals for microfabrication registration. In: Proc. 8th Int. Congr. Electr. Microsc. Australian Acad. Sci., Canberra, 650-651.

Christenhuss R, Reimer L (1969) Kontrast und Auflosungsvermogen an kantenformigen Objekten (Contrast and resolution of irregular samples). BEDO **2**, 89-100.

Cosslett VE, Thomas RN (1964) Multiple scattering of 5-30 keV electrons in evaporated metal films. II: Range energy relations. Brit. J. Appl: Phys. **15**, 1283-1300.

Cosslett VE, Thomas RN (1965) Multiple scattering of 5-30 keV electrons in evaporated metal films. III: Backscattering and absorption. Brit. J. Appl. Phys. **16**, 779-796.

Crewe AV, Isaacson M, Johnson D (1970) Secondary electron detection in a field emission scanning microscope. Rev. Sci. Instrum. **41**, 20-24.

Crewe AV, Lin PSD (1976) The use of backscattered electrons for imaging purposes in a scanning electron microscope. Ultramicroscopy **1**, 231-238.

Czyzewski Z, Kaczmarek D (1985) Backscattered electron signals from silicon marks: experiment and theory. BEDO **18**, 79-84.

Czyzewski Z, Joy DC (1991) Calculation of secondary electron production using a diffusion matrix. Scanning **13**, 227-232.

Darlinski A (1981) Measurement of angular distribution of the backscattered electrons in the energy range of 5 to 30 keV. Phys. Status Solidi (a) **63**, 663-667.

DeNee PB (1978) Measurement of mass and thickness of respirable size dust particles by SEM backscattered electron imaging. Scanning Electron Microsc. **1978**; I: 741-746.

Desai V, Reimer L (1990) Calculation of the signal of backscattered electrons using a diffusion matrix from Monte Carlo calculations. Scanning **12**, 1-4.

Ding ZJ, Shimizu R (1989) Theoretical study of the ultimate resolution of SEM. J. Microsc. **154**, 193-207.

Drescher H, Reimer L, Seidel H (1970) Rückstreukoeffizient und Sekundarelektronen-Ausbeute von 10-100 keV und Beziehungen zur Raster-Elektronenmikroskopie. (Backscatter coefficient and production of secondary electrons in the 10-100 keV range in relation to scanning electron microscopy). Z. angew. Physik **29**, 331 -336.

Endruschat FE, Börner M, Müller KH (1989) Limits of electron optical defect inspection of X-ray-lithography-masks. Microelectronic Eng. **9**, 401-404.

Everhart TE, Wells OC, Oatley CW (1959) Factors affecting contrast and resolution in the scanning electron microscope. J. Electron. Control **7**, 97-111.

Everhart TE, Thornley RFM (1960) Wide-band detector for micro-microampere low-energy electron currents. J. Sci. Instrum. **37**, 246-248.

Fitch RK, Johnson JD, Walker AR (1984) A "close approach" high-energy electron detector for examination of insulating materials in a scanning electron microscope. J. Phys. **E 17**, 25-27.

Frisova AA, Reimer L, Ushakov NG, Zaitsev SI (1991) Comparison of a simple model of BSE signal formation and surface reconstruction with Monte Carlo calculations. Scanning **13**, 363-368.

George EP, Robinson VNE (1975) Topographic intensity profiles in the scanning electron microscope-cubes. J. Microsc. **105**, 289-297.

George EP, Robinson VNE (1977) The influence of electron scattering on the detection of fine topographic detail in the scanning electron microscope (SEM). Scanning Electron Microsc. **1977**; I: 63-70.

Griffiths BW, Pollard P, Venables JA (1972) A channel plate detector for the scanning electron microscope. In: Proc. 5th Eur. Congr. Electr. Microsc. Inst. Physics, Bristol, U.K. 176-177.

Hasselbach F (1988) The emission microscope: a valuable tool for investigating the fundamentals of the scanning electron microscope. Scanning Microsc. **2**, 41-

56.

Hasselbach F, Rieke U (1976) Emission microscopical investigation of the edge brightening effect in scanning electron microscopy. In: Proc. 6th Eur. Congr. Electr. Microsc. Tal International, Jerusalem, 296-298.

Hatzakis M (1970) A new method of forming scintillators for electron collectors. Rev. Sci. Instrum. **41**, 128.

Heidenreich RD, Thompson LF (1973) Direct observation of backscatter electron distributions on surfaces. Appl. Phys. Lett. **22**, 279-81.

Heinrich KFJ (1966) Electron probe microanalysis by specimen current measurement. In: Proc. 4th Int. Congr. X-Ray opt. Microanal. Hermann, Paris. 159-167.

Hejna J (1987) A ring scintillation detector for detection of backscattered electrons in the scanning electron microscope. Scanning Microsc. **1**, 983-987.

Hejna J (1988) Optimization of the ring scintillation detector for backscattered electrons in the scanning electron microscope. In: EUREM 88. Inst. Phys. (Bristol) Conf. Ser. No. **93**(1). 119-120.

Hejna J, Radzimski Z, Buczkowski A (1985) Detection system for scanning electron microscope. Scanning Electron Microsc. **1985**; I: 151-156.

Hejna J, Reimer L (1987) Backscattered electron multidetector systems for improved quantitative topographic contrast. Scanning **2**, 162-172.

Hohn FJ, Kindt M, Niedrig H, Stuth B (1976) Elektronenrückstreumessungen an dünnen Schichten auf massiven Trägersubstanzen (Measurement of backscattered electrons in thin layers on massive substrates). Optik **46**, 491-500.

Hughes KA, Sulway DV, Wayte RC, Thornton PR (1967) Application of secondary-electron channel multipliers to scanning electron microscopy. J. Appl. Phys. **38**, 4922-4923.

Hunger HJ, Rogaschewski S (1986) A study of electron backscattering of thin films on substrates. Scanning **8**, 257-263.

Joy DC (1984) Beam interactions, contrast and resolution in the SEM. J. Microsc. **136**, 241-258.

Joy DC (1991) Contrast in high-resolution scanning electron microscope images. J. Microsc. **161**, 343-355.

Joy DC, Pawley JB (1992) High-resolution scanning electron microscopy. Ultramicroscopy **47**, 80-100.

Kanter H (1957) Zur Rückstreuung von Elektronen im Energiebereich von 10 bis 100 keV. (Electron backscatter in the energy range of 10-100 keV). Ann. Physik **20**, 144-166.

Kanter H (1961) Contribution of backscattered electrons to secondary electron formation. Phys. Rev. **121**, 681-684.

Kikuchi M, Takashima S (1978) Multi-purpose backscattered electron detector. In: Electron Microscopy 1978, Proc. 9th Int. Congr. Electr. Microsc. (Toronto), Microsc. Soc. Canada, Toronto, Vol. 1. 82-83.

Kimoto S, Hashimoto H, Kosuge T, Hert W (1965) Die Anwendung eines Mehrfach-Detektorsystems zur stereoskopischen Rasterbeobachtung in der Elektronenstrahl Mikroanalyse. (Use of a multiple detector system for stereo scanning imaging in electron probe microanalysis). Mikrochimica Acta, 471-478.

Kimoto S, Hashimoto H (1966) Stereoscopic observation in SEM using multiple detectors. In: The Electron Microprobe. McKinley TD (ed.). Wiley, New York. 480-489.

Koike H, Ueno K, Suzuki M (1971) Scanning device combined with conventional electron microscope. In: Proc. 29th EMSA Meeting. San Francisco Press. 28-29.

Kotera M (1989) A Monte Carlo simulation of primary and secondary electron trajectories in a specimen. J. Appl. Phys. **65**, 3991-3998.

Kotera M, Fujiwara T, Suga H, Wittry DB (1990) A simulation of the topographic contrast in the SEM. Jpn. J. Appl. Phys. **29**, 2312-2316.

Kuypers W, Lichtenegger S (1980) Universal detector system for backscattered electrons, transmitted electrons and cathodoluminescence. In: Electron Microscopy 1980, Proc. 7th Eur. Congr. Electr. Microsc. 7th Eur. Congr. Electr. Microsc. Found., Leiden, Vol. 1. 522-523.

Lange M, Reimer L, Tollkamp C (1984) Testing of detector strategies in scanning electron microscopy by isodensities. J. Microsc. **134**, 1-12.

Lebiedzik J (1979) An automatic topographical surface reconstruction in the SEM. Scanning **2**, 230-237.

Liu J, Cowley JM (1988) Contrast and resolution of electron images in a scanning transmission electron microscope. Scanning Microsc. **2**, 1957-1970.

Marshall DC, Stephen J (1972) Secondary electron detector, with an extended life, for use in a scanning electron microscope. J. Phys. **E 5**, 1046-1047.

Matsukawa T, Shimizu R (1974) A new type edge effect in high resolution scanning electron microscopy. Jpn. J. Appl. Phys. **13**, 583-586.

McMullan D (1953) The scanning electron microscope and the electron-optical examination of surfaces. Electronic Eng. **25**, 46-50.

Moll SH, Healey F, Sullivan B, Johnson W (1978) A high efficiency, nondirectional backscattered electron detection mode for SEM. Scanning Electron Microsc. **1978**; I: 303-310.

Munden AB, Walker DEY (1973) A silicon detector for the Stereoscan scanning electron microscope. J. Phys. **E 6**, 916-920.

Murata K, Kotera M, Nagami K (1980) Surface dis-

tribution of backscattered electrons in the SEM and EPMA. In: Proc. 8th Int. Congr. X-Ray Opt. Microanal. Beaman DR, Ogilvie RE, Wittry DB (eds.). Pendall Publ. Comp., Midland, MI (USA). 434-438.

Niedrig H (1982) Electron backscattering from thin films. J. Appl. Phys. **53**, R15-R49.

Niemietz A, Reimer L, Tollkamp C (1984) Analogue and digital reconstruction of the surface profile by the difference signal of two secondary electron detectors. In: Proc. 8th Europ. Congr. Electr. Microsc. Congr. Bureau Motesz, Budapest, Vol 1. 639-640.

Oatley CW (1981) Detectors for the scanning electron microscope. J. Phys. **E 14**, 971-976.

Oatley CW (1983) Electron currents in the specimen chamber of a scanning microscope. J. Phys. **E 16**, 308-312.

Ong PS (1970) Contrast and resolution in scanning electron microscopy using backscattered electrons. In: Proc. 28th EMSA Meeting. 392-393.

Palluel P (1947) Composante rediffusée du rayonnement electronique secondaire des metaux. (Backscatter component of secondary electron radiation in metals). C.R. Acad. Sci. **224**, 1492-1494.

Pawley JB (1974) Performance of SEM scintillation materials. Scanning Electron Microsc. **1974**, 27-34.

Peters KR (1982) Conditions required for high quality high magnification images in secondary electron-I scanning electron microscopy. Scanning Electron Microsc. **1982**; IV: 1359-1372.

Peters KR (1984) Generation, collection and properties of an SE-I enriched signal suitable for high resolution SEM on bulk specimens. In: Electron Beam Interactions with Solids. SEM Inc., AMF O'Hare (Chicago), IL. 363-372.

Radzimski ZJ, Russ JC (1989) Selection of backscattered electron energy for imaging in the scanning electron microscope. J. Computer-Assisted Microsc. **1**, 181-193.

Rajora OS, Curzon AE (1985) A simple method for determination of film thickness from electron image contrast in a scanning electron microscope. Thin Solid Films. **123**, 235-238.

Reimer L (1984) Electron signal and detector strategy. In: Electron Beam Interactions with Solids. SEM Inc., AMF O'Hare (Chicago), Il. 299-309.

Reimer L, Pfefferkorn G (1973) Raster-Elektronenmikroskopie. (Scanning electron microscopy). Springer Verlag. 39.

Reimer L, Riepenhausen M (1985) Detector strategy for secondary and backscattered electrons using multiple detector systems. Scanning **7**, 221-238.

Reimer L, Seidel H (1968) Messungen der Elektronenemission zur Deutung des Kontrastes im Raster-Elektronenmikroskop (Measurements of electron emission to interpret the contrast in the scanning electron microscope). In: Proc. 4th Eur. Reg. Conf. Electr. Microsc. Tipografia Poliglotta Vaticana, Rome. 79-80.

Reimer L, Stelter D (1987) Monte Carlo calculations of electron emission at surface edges. Scanning Microsc **1**, 951-962.

Reimer L, Volbert B (1979) Detector system for backscattered electrons by conversion to secondary electrons. Scanning **2**, 238-248.

Reimer L, Volbert B (1982) The origin and correction of SEM imaging artefacts arising from the use of the difference signal of two detectors. Philips Electron Optics Bulletin **118**, 6-9.

Reimer L, Popper W, Brocker W (1978) Experiments with a small solid angle detector for BSE. Scanning Electron Microsc. **1978**; I: 705-710.

Reimer L, Riepenhausen M, Tollkamp C (1984) Detector strategy for improvement of image contrast analogous to light illumination. Scanning 6, 155-167.

Reimer L, Riepenhausen M, Schierjott M (1986) Signal of backscattered electrons at edges and surface steps in dependence on surface tilt and take-off direction. Scanning **8**, 164-175.

Robinson VNE (1975) Backscattered electron imaging. Scanning Electron Microsc. **1975**; I: 51-60.

Robinson VNE, George EP (1976) Atomic number intensity profiles in the scanning electron microscope-gold and aluminium. J. Microsc. **107**, 85-91.

Rosenfield MG, Neureuther AR, Viswanathan R (1983) Simulation of backscattered electron signals for X-ray mask inspection. J. Vac. Sci. Technol. **B1**, 1358-1363.

Schauer P, Autrata R (1979) Electro-optical properties of a scintillation detector in SEM. J. Microsc. Spectrosc. Electron. **4**, 633-650.

Schauer P, Autrata R (1992) Light transport in single crystal scintillation detectors in SEM. Scanning **14**, 325-333.

Schur K, Schulte C, Reimer L (1967) Auflosungsvermogen und Kontrast von Oberflächenstufen bei der Abbildung mit einem Raster-Elektronenmikroskop (Stereoscan). (Resolution and contrast of surface steps in imaging by a scanning electron microscope (Stereoscan)). Z. angew. Phys. **23**, 405-412.

Secker PE, Rees A, Sanger CC (1973) Simple light pipes for the Stereoscan. J. Phys. **E 6**, 1090-1091.

Shiraki H, Aizaki N (1981) Backscattered electron signal from alignment mark: experiment and simulation. Jpn. J. Appl. Phys. **20**, L385-L388.

Stephani D (1979) Monte-Carlo calculations of backscattered electrons at registration marks. J. Vac. Sci. Technol. **16**, 1739-1742.

Takahashi R (1977) Backscattered SEM using CdS layer scintillator. Proposal of reflected SEM. Scanning

Electron Microsc. **1977**; I: 71-78.

Taylor ME (1972) An improved light pipe for the scanning electron microscope. Rev. Sci. Instrum. **43**, 1846-1847.

Uchikawa Y, Gouhara K, Yamada S, Ito T, Kodama T, Sardeshmukh P (1992) Comparative study of electron counting and conventional analogue detection of secondary electrons in SEM. J. Electr. Microsc. **41**, 253-260.

Volbert B (1982) Signal mixing techniques in scanning electron microscopy. Scanning Electron Microsc, **1982**; III: 897-905.

Volbert B, Reimer L (1980) Advantages of two opposite Everhart-Thornley detectors in SEM. Scanning Electron Microsc. **1980**; IV: 1-10.

Walker AR, Booker GR (1976) A simple energy filtering back-scattered electron detector. In: Developments in Electron Microscopy and Analysis, Proc. EMAG **75**. Academic Press. 119-122.

Wells OC (1970) New contrast mechanism for scanning electron microscope. Appl. Phys. Lett. **16**, 151-153.

Wells OC (1971) Low-loss image for surface scanning electron microscope. Appl. Phys. Lett. **19**, 232-235.

Wells OC (1977) Backscattered electron image (BSI) in the scanning electron microscope (SEM). Scanning Electron Microsc. **1977**; I: 747-771.

Wells OC (1978) Penetration effect at sharp edges in the scanning electron microscope. Scanning **1**, 58-62.

Wells OC (1979) Effects of collector take-off angle and energy filtering on the BSE image in the SEM. Scanning **2**, 199-216.

Wells OC (1986) Reduction of edge penetration effect in the scanning electron microscope. Scanning **8**, 120-126.

Wells OC (1988) Edge penetration effects in the low-loss electron image in the scanning electron microscope. In: Proc. 46th EMSA Meeting, 202-203.

Wells OC, Bremer CG (1970) Collector turret for scanning electron microscope. Rev. Sci. Instrum. **41**, 1034-1037.

Wells OC, Broers AN, Bremer CG (1973) Method for examining solid specimens with improved resolution in the scanning electron microscope (SEM). Appl. Phys. Lett. **23**, 353-355.

Wells OC, Bailey PJ (1985) Reduction of penetration effect at sharp edges in the scanning electron microscope (SEM). J. Microsc. **138**, RP3-RP4.

Wells OC, LeGoues FK, Hodgson RT (1990) Magnetically filtered low-loss scanning electron microscopy. Appl. Phys. Lett. **56**, 2351-2353.

Wells OC, Nacucchi M (1992) Secondary and backscattered electron emission in the scanning electron microscope - high resolution imaging. In: Proc. International School on Electron Microscopy in Material Science. Merli PG, Antisari MV (eds.), World Scientific, Singapore. 479-499.

Wittry DB (1966) Secondary electron emission in the electron probe. In: Proc. 4th Int. Congr. X-ray Opt. Microanal. Hermann, Paris. 168-180.

Wolf ED, Everhart TE (1969) Annular diode detector for high angular resolution pseudo-Kikuchi patterns. Scanning Electron Microsc. **1969**, 41-44.

Yamada S, Ito T, Gouhara K, Uchikawa Y (1991) Electron-count imaging in SEM. Scanning **13**, 165-171.

Discussion with Reviewers

K. Murata: As you showed, the sector-shaped ring detector is useful for obtaining good tilt contrast. Could you comment on the physical reason why this detector gives better results?

Author: Tilt contrast of a BSE detector depends mainly on the shape of the detector and on its position with respect to the specimen and the primary beam. Good tilt contrast obtained with the sector-shaped ring detector on uncoated specimens is a result of an optimization of these factors. The detector also gives good contrast on coated specimens. In this case, the change of the signal is additionally influenced by the change of a layer thickness, penetrated by primary electrons, with a tilt angle. As a result, the contrast is even better than for uncoated specimens and the signal rises to the tilt of 90°.

K. Murata: Most of the scanning electron micrographs are shown at 20 and 30 keV. Did you obtain similar conclusions, concerning tilt contrast, at lower energies also?

Author: Conclusions presented in the paper are valid for a primary beam energy higher than about 5 keV. Below this energy, origins of tilt contrast change (mainly for SE). As the primary beam energy is lowered, SE yield becomes less dependent on the tilt angle, and tilt contrast obtained with SE becomes weaker. Tilt contrast of BSE detectors remains similar to that at higher energies and good tilt contrast can be obtained with the ring detector. Results for low-voltage SEM will be published in the near future in other papers [J. Hejna. Backscattered electron imaging in low-voltage SEM. In: Proc. 13th Int. Congr. Electr. Microsc., (Paris) Les Editions de Physique, Les Ulis, Vol. 1, 75-76); J. Hejna. Topographic and material contrast in low-voltage SEM. (In preparation)].